Thin-Walled Structures 178 (2022) 109532

Contents lists available at ScienceDirect

Thin-Walled Structures

journal homepage: www.elsevier.com/locate/tws

Full length article

# Applicability and limitations of Donnell shell theory for vibration modelling of double-walled carbon nanotubes

Matteo Strozzi [a,b,*], Isaac E. Elishakoff [c], Leonid I. Manevitch [d], Oleg V. Gendelman [b]

[a] Department of Sciences and Methods for Engineering, University of Modena and Reggio Emilia, Via Giovanni Amendola 2, 42122, Reggio Emilia, Italy
[b] Faculty of Mechanical Engineering, Technion Israel Institute of Technology, Haifa, Israel
[c] Department of Ocean and Mechanical Engineering, Florida Atlantic University, Boca Raton (Florida), USA
[d] N.N. Semenov Institute of Chemical Physics, Russian Academy of Sciences, Moscow, Russia

ARTICLE INFO

*Keywords:*
Carbon nanotubes
Double-walled
Vibration modelling
Donnell shell theory
Natural frequencies

ABSTRACT

In this paper, the comparison is conducted between two shell theories as applied to the vibrations of double-walled carbon nanotubes (DWCNTs); specifically, the evaluation of the natural frequencies is conducted via Donnell and Sanders shell theories. The discrete DWCNTs are modelled by means of couples of concentric continuous circular cylindrical shells, where van der Waals interaction forces between the two shells are modelled via He's formulation. In order to take into account the chirality of DWCNTs, an anisotropic elastic shell model is used. Simply supported, clamped and free boundary conditions are applied and Rayleigh–Ritz method is adopted to obtain approximate natural frequencies and mode shapes. At the beginning, comparisons with experimental and molecular dynamics data are made, from which it is confirmed that anisotropic elastic shell model is more accurate than isotropic one and it is obtained that Sanders shell theory is more accurate than Donnell one. Then, a parametric analysis considering different values of aspect ratio and numbers of waves along the longitudinal and circumferential directions is carried out in the framework of the anisotropic elastic shell model. From these simulations, it is found that Donnell shell theory yields unsatisfactory results for relatively low numbers of longitudinal and circumferential waves, and for relatively high values of aspect ratio, with respect to Sanders shell theory. Therefore Donnell shell theory cannot be used for vibration modelling of DWCNTs in a large range of longitudinal and circumferential wavenumbers and aspect ratios.

## 1. Introduction

Research in nanotechnology attracted numerous investigators in last years. Recent status is reported in the monographs written by Elishakoff et al. [1], Chakraverty and Behera [2] and Liew et al. [3], as well as in the volumes edited by Tserpes and Silvestre [4] and Harik [5], for example.

Carbon nanotubes (CNTs) are used as ultrahigh frequency resonators in a very large number of nano-electro-mechanical devices such as sensors, oscillators, charge detectors and field emission devices [6,7]. Size reduction and stiffness increment of nano-mechanical resonators magnify their resonant frequencies and decrease their energy consumption, therefore improving their sensitivity.

Many experiments were performed on single-walled carbon nanotubes (SWCNTs) [8–10]. In these works, the linear vibrations of free–free SWCNTs are considered by using the resonant Raman spectroscopy with laser excitation wavelengths in the range of nanometres. Many Raman peaks are observed, which correspond to the vibrational modes of SWCNTs, where SWCNT chirality can be univocally assigned by measuring the natural frequency of the radial breathing mode (RBM), which is the lowest frequency axisymmetric mode, and then applying the theory of resonant transitions.

Because of their nanoscale size, it is very difficult to investigate the mechanical properties of SWCNTs by adopting experimental techniques, which require high resolution transmission electron microscopes and do not allow the natural frequencies of the different vibration modes to be easily separated within the frequency spectrum.

On the other hand, it was found that molecular dynamics (MD) simulations provide good predictions of mechanical behaviours of SWCNTs and multi-walled carbon nanotubes (MWCNTs) under external forces, with results close to the experimental ones [11–13]. In these works, natural frequencies of RBMs and beam-like modes (BLMs) considering CNTs with different geometries, boundary conditions and chirality are computed adopting molecular mechanics (MM) potential.

However, it was verified that the MD simulations are computationally inefficient, especially when dealing with MWCNTs that incorporate a large number of atoms. Therefore, more efficient analytical and

* Corresponding author at: Department of Sciences and Methods for Engineering, University of Modena and Reggio Emilia, Via Giovanni Amendola 2, 42122, Reggio Emilia, Italy.
*E-mail address:* matteo.strozzi@unimore.it (M. Strozzi).

https://doi.org/10.1016/j.tws.2022.109532
Received 16 April 2021; Received in revised form 21 May 2022; Accepted 25 May 2022
Available online xxxx
0263-8231/

numerical methods were developed to analyse classes of CNTs in a simpler way.

Such methods are generally based on continuous elastic models for the nanotube that allow a strong reduction of the number of degrees of freedom, at the same time correctly predicting static buckling and free vibration behaviour of CNTs obtained from experiments and MD simulations.

In particular, carbon nanotubes were modelled by researchers as Euler–Bernoulli beams [14–18], Timoshenko–Ehrenfest beams [19–23] and thin circular cylindrical shells [24–38]. In the latter respect, the relevant question arises: "Which thin shell theory should be applied to properly model carbon nanotube vibrations?"

The reference text on vibrations of circular cylindrical shells is represented by Leissa's book [39]. In this work, the equations of the most important thin shell theories (i.e., Donnell–Mushtari, Goldenveizer–Novozhilov, Flügge–Byrne–Lur'ye, Sanders–Koiter), together with the corresponding equations of motion and natural frequencies for circular cylindrical shells under different boundary conditions are reported. Readers interested in deepening vibrations of circular cylindrical shells and thin shell theories can refer to the books of Soedel [40], Ventsel [41] and Amabili [42].

Several papers on accuracy and limitations of thin shell theories in vibration modelling of circular cylindrical shells can be found. Amabili [43] compared the natural frequencies of circular cylindrical shells computed by considering four different thin shell theories, specifically Donnell–Mushtari, Sanders–Koiter, Flügge–Lur'ye–Byrne and Goldenveizer–Novozhilov, with the results of the elasticity theory. He demonstrated that the latter three thin shell theories provide more accurate results than the former one; in particular, he concluded that Donnell–Mushtari thin shell theory "... is accurate only for modes with circumferential wavenumber $n$ that is not small: specifically, $1/n^2 << 1$ must be satisfied, so that $n \geq 4$ or 5 is required in order to have fairly good accuracy". Lee and Kwak [44] compared the natural frequencies of circular cylindrical shells obtained by adopting six different thin shell theories, i.e., Donnell–Mushtari, Sanders–Koiter, Flügge–Byrne–Lur'ye, Love–Timoshenko, Reissner–Naghdi–Berry and Vlasov, with the results of FE analyses. By investigating only modes with relatively low circumferential wavenumber $n = (1,2)$ they found that, by increasing the aspect ratio $L/R$, Donnell–Mushtari thin shell theory loses its accuracy, while there are no evident differences among the other five shell theories. Farshidian and Oliazad [45] compared the natural frequencies of circular cylindrical shells calculated by means of ten different thin shell theories, i.e., Donnell–Mushtari, Love–Timoshenko, Arnold–Warburton, Houghton–Johns, Flügge–Byrne–Lur'ye, Sanders–Koiter, Kennard-Simplified, Reissner–Naghdi–Berry, Vlasov and Soedel, with experimental results. By considering a relatively low aspect ratio value $L/R \approx 20$ and modes with circumferential wavenumber $n = (2,3)$, they obtained that Donnell–Mushtari thin shell theory is not accurate for the longitudinal wavenumber $m = 1$–5, while the other thin shell theories, except for Houghton–Johns one, reveal very similar results. Hoff [46] compared the natural frequencies of circular cylindrical shells calculated by considering Donnell–Mushtari and Flügge–Byrne–Lur'ye thin shell theories; from these comparisons, he derived that, for sufficiently thin shells with thickness ratio $R/h = 50$, Donnell–Mushtari shell theory for the longitudinal wavenumber $m = 1$ is accurate enough in case of aspect ratio $L/R < 30$ while, for $m > 1$, the accuracy is always better than for $m = 1$; in addition, he found that Donnell–Mushtari thin shell theory gives accurate results when the circumferential wavenumber $n$ is sufficiently large, i.e. $n \geq 4$, while the error is very large for $n \leq 3$. Hashemi et al. [47] identified the validity range of Donnell and Sanders shell theories for the vibration analysis of functionally graded circular cylindrical shell panels by means of comparisons with the results of FE analyses; with respect to the fundamental natural frequency of the panel, they obtained that the difference between the theories increases with increasing the aspect ratio $L/R$ and moving from simply supported to free boundary conditions.

Conversely, only a few papers on accuracy and limitations of thin shell theories in vibration modelling of single-walled carbon nanotubes (SWCNTs) are available. Wang et al. [48] examined applicability and limitations of Donnell–Mushtari thin shell theory for the investigation of the free vibrations of SWCNTs compared to Flügge–Byrne–Lur'ye thin shell theory. They obtained that the natural frequencies of the axisymmetric modes ($n = 0$) are in very close agreement for sufficiently thin layers (ratio $h/R << 1$) for every value of longitudinal wavenumber $m$ and aspect ratio $L/R$; the relative error obtained by Donnell–Mushtari thin shell theory decreases with decreasing the axial wavelength $L/(Rm)$ and with increasing the circumferential wavenumber $n$: these results show that the largest error occurs when $n = 1$ (beam-like vibrations) and $L/(Rm)$ is relatively high, that is the case when vibration modes of long SWCNTs with $m = 1$ are analysed. Other studies on the accuracy of Donnell–Mushtari shell theory in vibration modelling of SWCNTs are reported in Refs. [49–51].

CNTs are frequently modelled as isotropic elastic shells. However, there are clear indications showing that CNTs exhibit chirality-induced anisotropic behaviour that cannot be neglected [52]. Chang et al. [53] developed a molecular mechanics model, called "stick-spiral model", able to predict chirality and size-dependent elastic properties of SWCNTs. Starting from the governing equations of this model, they derived the explicit expression for longitudinal Young's modulus and Poisson's ratio, circumferential Young's modulus and Poisson's ratio, and tangential shear modulus in the case of chiral SWCNTs. In particular, they demonstrated that the classical relationship of the isotropic elastic continuum mechanics between Young's and shear moduli is no longer valid for SWCNTs. Chang [54] derived a closed-form expression for the anisotropic surface elastic constants of SWCNTs obtained via the "stick-spiral model" of Ref. [53], and developed a molecular based anisotropic shell model able to predict the mechanical behaviour of SWCNTs. In particular, by adopting Donnell thin shell theory, he obtained explicit expressions for the coupling of axial, circumferential and torsional deformations, radial breathing mode natural frequency, and longitudinal and torsional wave speed. Ghavanloo and Fazelzadeh [55,56], starting from the results of [54], developed an anisotropic elastic shell model including chirality effects to study the vibration characteristics of SWCNTs. By applying Flügge thin shell theory and complex method, they obtained natural frequencies of radial breathing, torsional, longitudinal and radial modes under different CNT diameters and chiralities. They validated their model by means of comparisons with experimental RRS and numerical MD simulation data.

From Refs. [48–51] it was demonstrated that the accuracy of Donnell shell theory in vibration modelling of SWCNTs varies by varying aspect ratios and wavenumbers, and from Refs. [52–56] it was established that an anisotropic elastic shell model must be adopted in order to take into account SWCNT chirality: the aim of the present paper is, therefore, to extend the previously obtained results for SWCNTs by considering, in the framework of an anisotropic elastic shell model, applicability and limitations of Donnell shell theory in vibration modelling of DWCNTs.

Very relevant results for the present paper, obtained via molecular dynamics simulations, were reported by Zhang and Shen. In particular, in Ref. [57] they demonstrated that the material properties of SWCNTs are size-dependent, i.e., they depend on CNT radius: from this result, it follows that, in the case of DWCNTs, as in the present paper, the material properties should be different for the inner and outer SWCNT. In Ref. [58] they obtained that the elastic moduli of the inner tube in a DWCNT are indeed larger than those of the outer one, but their difference is very small, and the two SWCNTs can be assumed to have the same values of elastic moduli with reasonable accuracy.

In this paper, an anisotropic elastic shell model is adopted to analyse the vibrations of simply supported, clamped and free DWCNTs. Donnell and Sanders shell theories are used to obtain elastic strain and kinetic energies. He's formulation is considered to model van der Waals interaction forces between the two concentric SWCNTs. The displacement field of each SWCNT is expanded by means of a double mixed

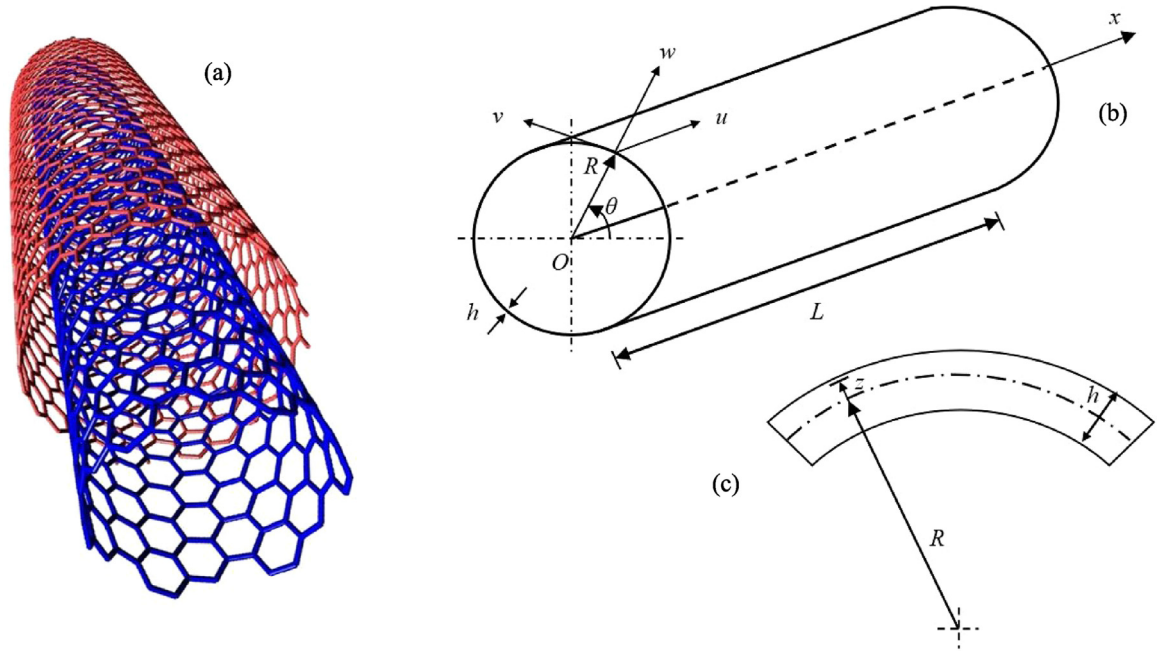


**Fig. 1.** Continuum modelling of a DWCNT. (a) Actual discrete DWCNT. (b) Geometry of the equivalent continuous thin circular cylindrical shell. (c) Cross-section of the surface of the equivalent continuous shell.

series in terms of Chebyshev orthogonal polynomials and harmonic functions along the longitudinal and circumferential direction, respectively. Rayleigh–Ritz method is adopted in order to obtain approximate natural frequencies and corresponding modal shapes. In the numerical results, at the beginning, natural frequencies of SWCNTs obtained adopting isotropic and anisotropic elastic shell models and considering Sanders shell theory are compared with experimental data from resonant Raman spectroscopy available in the literature in order to verify the higher accuracy of the anisotropic model. Then, natural frequencies of SWCNTs obtained adopting Donnell and Sanders shell theories and considering the anisotropic elastic shell model are compared with numerical data from molecular dynamics simulations available in the literature in order to verify the higher accuracy of Sanders shell theory. Starting from these results, considering an anisotropic elastic shell model, natural frequencies of DWCNTs with different aspect ratios and numbers of waves along longitudinal and circumferential directions obtained by adopting Donnell and Sanders shell theories are compared. By assuming the more accurate Sanders shell theory as a reference, applicability and limitations of Donnell shell theory for vibration modelling of DWCNTs are investigated. At the end, the previous numerical results for simply supported DWCNTs are justified analytically by considering applicability and limitations of Donnell shell theory in vibration modelling of simply supported thin cylindrical shells of finite length.

## 2. Donnell and Sanders shell theories for DWCNTs

In the present paper, the actual discrete DWCNT of Fig. 1(a) is modelled by means of a couple of concentric equivalent continuous elastic thin cylindrical shells with van der Waals interaction forces. In Fig. 1(b, c) a continuous elastic thin cylindrical shell with radius $R$, length $L$ and thickness $h$ is shown; a cylindrical coordinate system $(O, x, \theta, z)$ is considered, where the origin $O$ of the reference system is located at the centre of one end of the cylindrical shell. Three displacements are present: longitudinal $u(x, \theta, t)$, circumferential $v(x, \theta, t)$ and radial $w(x, \theta, t)$, where the radial displacement $w$ is assumed as positive outward; $(x, \theta)$ are the longitudinal and angular coordinates of an arbitrary point on the middle surface of the shell; $z$ is the radial coordinate along the thickness $h$; $t$ is the time.

### 2.1. Displacement field

A relevant issue in CNT continuum modelling is given by the infinitesimal dimensions, which can give rise to very fast time scales and therefore to very hard convergence problems in the numerical integration; to avoid these problems, in this work, all dimensionless parameters are considered.

The dimensionless displacement field $(\tilde{u}_i, \tilde{v}_i, \tilde{w}_i)$ of the $i$th cylindrical shell is written as [29]:

$$\tilde{u}_i = \frac{u_i}{R_i} \qquad \tilde{v}_i = \frac{v_i}{R_i} \qquad \tilde{w}_i = \frac{w_i}{R_i} \qquad i = 1, 2 \tag{1}$$

where $(u_i, v_i, w_i)$ is the dimensional displacement field and $R_i$ is the radius of the $i$th shell.

### 2.2. Strain–displacement relationships

In this paper, Donnell and Sanders shell theories are used to model DWCNT dynamics.

The linear relationships between strains and displacements in these two shell theories are based on "Love's first approximation" assumptions [39]: (i) the thickness of the shell $h$ is small if compared with the other shell dimensions, for example the radius of curvature of the middle surface $R$ and the length $L$, (ii) strains and displacements are sufficiently small so that the quantities of the second and higher-order magnitude into the strain–displacement relationships may be neglected in comparison with the first-order terms, (iii) the transverse normal stress is small with respect to the other normal stress components and may be neglected (i.e. $\sigma_z = 0$), (iv) normals to the undeformed middle surface remain straight and normal to the deformed middle surface and suffer no extension ("Kirchhoff's kinematic hypothesis").

As for the first geometric assumption, with regard to the thickness-to-radius ratio $h/R$, it was proven that the range of validity of the thin shell theories, e.g. Donnell and Sanders shell theories, is given by $0.002 \leq h/R \leq 0.05$, see Ref. [42] for more details.

The consequence of the last geometric assumption is that the transverse shear strains of the circular cylindrical shell may be neglected (i.e. $\gamma_{xz} = \gamma_{\theta z} = 0$); in addition, also the rotary inertia of the shell is neglected.

According to Donnell and Sanders shell theories, the dimensionless middle surface strains of the $i$th cylindrical shell $(\tilde{\varepsilon}_{x,0,i}, \tilde{\varepsilon}_{\theta,0,i}, \tilde{\gamma}_{x\theta,0,i})$ are written in linear field as [29]:

$$\tilde{\varepsilon}_{x,0,i} = \alpha_i \frac{\partial \tilde{u}_i}{\partial \eta} \qquad \tilde{\varepsilon}_{\theta,0,i} = \frac{\partial \tilde{v}_i}{\partial \theta} + \tilde{w}_i \qquad \tilde{\gamma}_{x\theta,0,i} = \frac{\partial \tilde{u}_i}{\partial \theta} + \alpha_i \frac{\partial \tilde{v}_i}{\partial \eta} \qquad i = 1,2 \tag{2}$$

where $\eta = x/L$ is the dimensionless longitudinal coordinate of the shell and $\alpha_i = R_i/L$.

According to Donnell and Sanders shell theories, the dimensionless middle surface changes in curvature and torsion of the $i$th cylindrical shell $(\tilde{k}_{x,i}, \tilde{k}_{\theta,i}, \tilde{k}_{x\theta,i})$ are written as [29]:

$$\begin{aligned} &\tilde{k}_{x,i} = -\alpha_i^2 \frac{\partial^2 \tilde{w}_i}{\partial \eta^2} \qquad \tilde{k}_{\theta,i} = \varphi \frac{\partial \tilde{v}_i}{\partial \theta} - \frac{\partial^2 \tilde{w}_i}{\partial \theta^2} \\ &\tilde{k}_{x\theta,i} = -2\alpha_i \frac{\partial^2 \tilde{w}_i}{\partial \eta \partial \theta} + \frac{\varphi}{2}\left(3\alpha_i \frac{\partial \tilde{v}_i}{\partial \eta} - \frac{\partial \tilde{u}_i}{\partial \theta}\right) \quad i = 1,2 \end{aligned} \tag{3}$$

In Eqs. (3), an artificial control parameter $\varphi$ is introduced, allowing for the application of both Sanders and Donnell shell theory; in particular, by imposing $\varphi = 1$ Sanders shell theory is adopted, while by imposing $\varphi = 0$ Donnell shell theory is adopted. The introduction of the control parameter $\varphi$ is particularly useful because it allows the computational implementation of the two theories by adopting the same equations and varying only the value of the parameter. Moreover, from Eqs. (3), it can be noted that the control parameter $\varphi$ is present only in the dimensionless middle surface change in curvature along the angular coordinate $\theta$ and in the dimensionless middle surface torsion in the plane $(x, \theta)$, since these two terms are the only responsible for the differences in the natural frequencies between Donnell and Sanders shell theories.

According to Donnell and Sanders shell theories, the dimensionless strain components at an arbitrary point of the $i$th shell $(\tilde{\varepsilon}_{x,i}, \tilde{\varepsilon}_{\theta,i}, \tilde{\gamma}_{x\theta,i})$ are related to the dimensionless middle surface strains and changes in curvature and torsion of the $i$th shell by means of the following relationships [29]:

$$\begin{aligned} &\tilde{\varepsilon}_{x,i} = \tilde{\varepsilon}_{x,0,i} + \zeta_i \tilde{k}_{x,i} \qquad \tilde{\varepsilon}_{\theta,i} = \tilde{\varepsilon}_{\theta,0,i} + \zeta_i \tilde{k}_{\theta,i} \\ &\tilde{\gamma}_{x\theta,i} = \tilde{\gamma}_{x\theta,0,i} + \zeta_i \tilde{k}_{x\theta,i} \quad i = 1,2 \end{aligned} \tag{4}$$

where $\zeta_i = z_i/R_i$ is the dimensionless radial coordinate of the $i$th cylindrical shell.

## 3. Anisotropic elastic shell model for DWCNTs

Another relevant issue in CNT continuum modelling is represented by the choice of the elastic shell model; indeed, CNTs are discrete systems, i.e. they are intrinsically non-isotropic. Since it was proven that the use of an isotropic model can lead to relevant errors in CNT vibration analysis, see Ref. [52], then in the present paper an anisotropic elastic shell model for DWCNT vibration analysis is adopted.

### 3.1. Stress–strain relationships

In anisotropic elasticity, by assuming the plane stress hypothesis ($\sigma_z = 0$), the dimensionless stresses $(\tilde{\sigma}_{x,i}, \tilde{\sigma}_{\theta,i}, \tilde{\tau}_{x\theta,i})$ of the $i$th cylindrical shell are related to the corresponding dimensionless strains by means of the following constitutive equations [55]:

$$\begin{aligned} &\tilde{\sigma}_{x,i} = \tilde{Y}_{11,i}\tilde{\varepsilon}_{x,i} + \tilde{Y}_{12,i}\tilde{\varepsilon}_{\theta,i} + \tilde{Y}_{13,i}\tilde{\gamma}_{x\theta,i} \\ &\tilde{\sigma}_{\theta,i} = \tilde{Y}_{21,i}\tilde{\varepsilon}_{x,i} + \tilde{Y}_{22,i}\tilde{\varepsilon}_{\theta,i} + \tilde{Y}_{23,i}\tilde{\gamma}_{x\theta,i} \qquad i = 1,2 \\ &\tilde{\tau}_{x\theta,i} = \tilde{Y}_{31,i}\tilde{\varepsilon}_{x,i} + \tilde{Y}_{32,i}\tilde{\varepsilon}_{\theta,i} + \tilde{Y}_{33,i}\tilde{\gamma}_{x\theta,i} \end{aligned} \tag{5}$$

where the dimensionless parameters $\tilde{Y}_{jk,i}$ are anisotropic surface elastic constants, in the form [55]:

$$\tilde{Y}_{jk,i} = \left(\tilde{G}_{lj,i}\tilde{G}_{lk,i} + 2\mu\tilde{H}_{lj,i}\tilde{H}_{lk,i}\right) \qquad j,k,l = 1,2,3 \text{ (sum over } l) \qquad i = 1,2 \tag{6}$$

where $(\tilde{G}_{lj,i}, \tilde{G}_{lk,i}, \tilde{H}_{lj,i}, \tilde{H}_{lk,i})$ are dimensionless constants and $\mu$ is a dimensionless parameter [56]:

$$\mu = \frac{K_\theta}{K_\rho a^2} \tag{7}$$

where $K_\rho$ and $K_\theta$ are force constants associated with stretching and angular distortion of the carbon–carbon bond, respectively, and $a$ is the carbon–carbon (C-C) bond length. The force constants $K_\rho$ and $K_\theta$ can be derived from quantum or empirical molecular mechanics analyses, or fitted to experimental data, see Ref. [53] for more details.

The corresponding matrices $\tilde{\mathbf{G}}_i$ and $\tilde{\mathbf{H}}_i$ can be calculated as follows [56]:

$$\tilde{\mathbf{G}}_i = \tilde{\mathbf{B}}_i^{-1}\left(\tilde{\mathbf{I}} - \tilde{\mathbf{D}}_i\tilde{\mathbf{F}}_i\right), \qquad \tilde{\mathbf{H}}_i = \tilde{\mathbf{Q}}_i\tilde{\mathbf{F}}_i \quad i = 1,2 \tag{8}$$

where $\tilde{\mathbf{I}}$ is the identity matrix, matrix $\tilde{\mathbf{F}}_i$ is given by [55]:

$$\tilde{\mathbf{F}}_i = \left[\tilde{\mathbf{U}}_i\tilde{\mathbf{B}}_i^{-1}\tilde{\mathbf{D}}_i - (2\mu\tilde{\mathbf{V}}_i\tilde{\mathbf{A}}_i + \tilde{\mathbf{W}}_i)\right]^{-1}\tilde{\mathbf{U}}_i\tilde{\mathbf{B}}_i^{-1} \quad i = 1,2 \tag{9}$$

and matrices $\left(\tilde{\mathbf{A}}_i, \tilde{\mathbf{B}}_i, \tilde{\mathbf{D}}_i, \tilde{\mathbf{U}}_i, \tilde{\mathbf{V}}_i, \tilde{\mathbf{W}}_i, \tilde{\mathbf{Q}}_i\right)$ are given by [55]:

$$\begin{aligned} &\tilde{\mathbf{A}}_i = \left\{\tilde{A}_{jk,i}\right\} = \left\{-\cos\omega_{jp,i}\cos\omega_{kp,i}\right\} \\ &j,k,p = 1,2,3 \text{ (sum over } p) \quad i = 1,2 \end{aligned} \tag{10}$$

$$\tilde{\mathbf{B}}_i = \frac{1}{3\sqrt{r_i^2 + r_i s_i + s_i^2}} \times \begin{pmatrix} (2r_i + s_i)\cos\phi_{1,i} & -(r_i - s_i)\cos\phi_{2,i} & -(r_i + 2s_i)\cos\phi_{3,i} \\ \sqrt{3}s_i\sin\phi_{1,i} & -\sqrt{3}(r_i - s_i)\sin\phi_{2,i} & \sqrt{3}r_i\sin\phi_{3,i} \\ (2r_i + s_i)\sin\phi_{1,i} & -(r_i - s_i)\sin\phi_{2,i} & -(r_i + 2s_i)\sin\phi_{3,i} \end{pmatrix} \tag{11}$$

$$\tilde{\mathbf{D}}_i = \frac{1}{3\sqrt{r_i^2 + r_i s_i + s_i^2}} \times \begin{pmatrix} -(2r_i + s_i)\sin\phi_{1,i} & (r_i - s_i)\sin\phi_{2,i} & (r_i + 2s_i)\sin\phi_{3,i} \\ \sqrt{3}s_i\cos\phi_{1,i} & -\sqrt{3}(r_i + s_i)\cos\phi_{2,i} & \sqrt{3}r_i\cos\phi_{3,i} \\ (2r_i + s_i)\cos\phi_{1,i} & -(r_i - s_i)\cos\phi_{2,i} & -(r_i + 2s_i)\cos\phi_{3,i} \end{pmatrix} \tag{12}$$

$$\tilde{\mathbf{U}}_i = \begin{pmatrix} \sin\phi_{1,i} & \sin\phi_{2,i} & \sin\phi_{3,i} \\ \cos\phi_{1,i} & \cos\phi_{2,i} & \cos\phi_{3,i} \\ s_i\cos\phi_{1,i} & -(r_i + s_i)\cos\phi_{2,i} & r_i\cos\phi_{3,i} \end{pmatrix} \tag{13}$$

$$\tilde{\mathbf{V}}_i = \begin{pmatrix} -\cos\phi_{1,i} & -\cos\phi_{2,i} & -\cos\phi_{3,i} \\ \sin\phi_{1,i} & \sin\phi_{2,i} & \sin\phi_{3,i} \\ 0 & 0 & 0 \end{pmatrix} \tag{14}$$

$$\tilde{\mathbf{W}}_i = \begin{pmatrix} 0 & 0 & 0 \\ 0 & 0 & 0 \\ -s_i\sin\phi_{1,i} & (r_i + s_i)\sin\phi_{2,i} & -r_i\sin\phi_{3,i} \end{pmatrix} \tag{15}$$

$$\tilde{\mathbf{Q}}_i = \left\{\tilde{Q}_{jk,i}\right\} = \left\{-\cos\omega_{kj,i}\right\} \quad j,k = 1,2,3 \quad i = 1,2 \tag{16}$$

where [55]:

$$\cos\omega_{jk,i} = \begin{cases} (\cos\phi_{j,i}\sin\phi_{p,i}\cos\varphi_{k,i} - \sin\phi_{j,i}\cos\phi_{p,i})/\sin\theta_{k,i} & j \neq k \neq p \\ 0 & j = k \end{cases} \tag{17}$$

and $(r_i, s_i)$ are the chirality indices of the $i$th carbon nanotube, which define its radius [25]:

$$R_i = \frac{\sqrt{3}a}{2\pi}\sqrt{r_i^2 + r_i s_i + s_i^2} \tag{18}$$

The structural parameters of the $i$th SWCNT, i.e., chiral angles $(\phi_{1,i}, \phi_{2,i}, \phi_{3,i})$ and torsion angles $(\varphi_{1,i}, \varphi_{2,i}, \varphi_{3,i})$, which can be calculated by means of the equations [54]:

$$\phi_{1,i} = \arccos\frac{2r_i + s_i}{2\sqrt{r_i^2 + r_i s_i + s_i^2}} \qquad \phi_{2,i} = \frac{4\pi}{3} + \phi_{1,i} \qquad \phi_{3,i} = \frac{2\pi}{3} + \phi_{1,i} \tag{19}$$

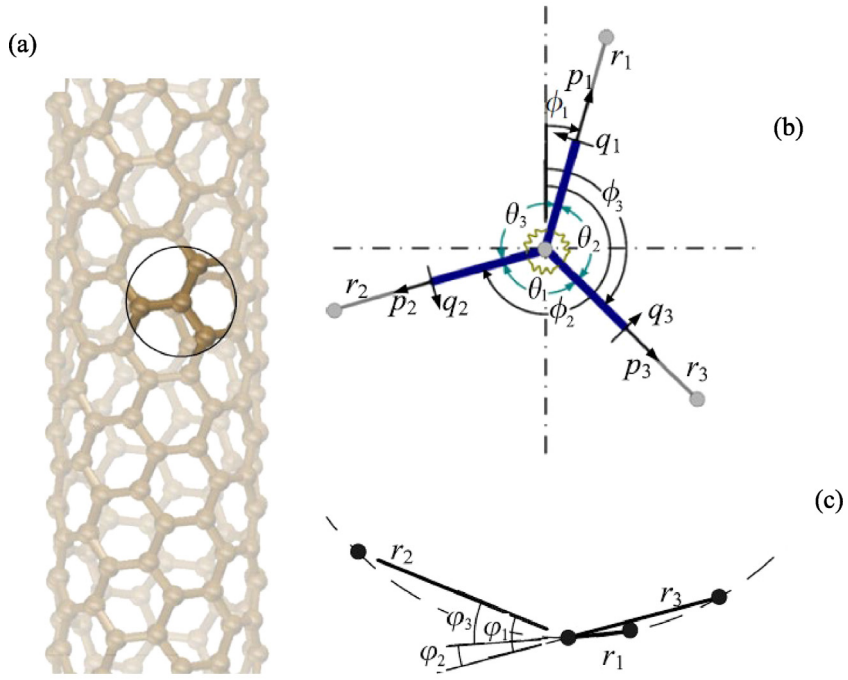


**Fig. 2.** Schematic illustration of a $(r, s)$ single-walled carbon nanotube. (a) Global structure with a zoom of a single representative atom; (b) side view of the local structure; (c) top view of the local structure [54].

$$\varphi_{1,i} = \frac{\pi}{\sqrt{r_i^2 + r_i s_i + s_i^2}} \cos\phi_{1,i} \qquad \varphi_{2,i} = \frac{\pi}{\sqrt{r_i^2 + r_i s_i + s_i^2}} \cos\left(\frac{\pi}{3} + \phi_{1,i}\right)$$
$$\varphi_{3,i} = \frac{\pi}{\sqrt{r_i^2 + r_i s_i + s_i^2}} \cos\left(\frac{\pi}{3} - \phi_{1,i}\right) \tag{20}$$

and bond angles $(\theta_{1,i}, \theta_{2,i}, \theta_{3,i})$, which are written in following form [54]:

$$\cos\theta_{j,i} = \sin\phi_{k,i} \sin\phi_{p,i} \cos\varphi_{j,i} + \cos\phi_{k,i} \cos\phi_{p,i}$$
$$j,k,p = 1,2,3 \text{ (sum over } p) \quad i = 1,2 \tag{21}$$

are illustrated in Fig. 2, see Ref. [54] for more details.

It should be underlined that, in the anisotropic elastic constitutive equations (5), the chirality effects are considered by adopting the anisotropic surface elastic constants $\tilde{Y}_{jk,i}$.

### 3.2. Force and moment resultants

Starting from the anisotropic elastic constitutive equations (5), the corresponding dimensionless force resultants per unit length of the $i$th cylindrical shell $(\tilde{N}_{x,i}, \tilde{N}_{\theta,i}, \tilde{N}_{x\theta,i})$ can be written as a function of the corresponding dimensionless middle surface strains in the form:

$$\tilde{N}_{x,i} = \tilde{Y}_{11,i}\tilde{\varepsilon}_{x,0,i} + \tilde{Y}_{12,i}\tilde{\varepsilon}_{\theta,0,i} + \tilde{Y}_{13,i}\tilde{\gamma}_{x\theta,0,i}$$
$$\tilde{N}_{\theta,i} = \tilde{Y}_{21,i}\tilde{\varepsilon}_{x,0,i} + \tilde{Y}_{22,i}\tilde{\varepsilon}_{\theta,0,i} + \tilde{Y}_{23,i}\tilde{\gamma}_{x\theta,0,i} \tag{22}$$
$$\tilde{N}_{x\theta,i} = \tilde{Y}_{31,i}\tilde{\varepsilon}_{x,0,i} + \tilde{Y}_{32,i}\tilde{\varepsilon}_{\theta,0,i} + \tilde{Y}_{33,i}\tilde{\gamma}_{x\theta,0,i}$$

and the dimensionless moment resultants per unit length of the $i$th cylindrical shell $(\tilde{M}_{x,i}, \tilde{M}_{\theta,i}, \tilde{M}_{x\theta,i})$ can be written as a function of the corresponding dimensionless middle surface changes in curvature and torsion in the form:

$$\tilde{M}_{x,i} = \frac{\beta_i}{12}\left(\tilde{Y}_{11,i}\tilde{k}_{x,i} + \tilde{Y}_{12,i}\tilde{k}_{\theta,i} + \tilde{Y}_{13,i}\tilde{k}_{x\theta,i}\right)$$
$$\tilde{M}_{\theta,i} = \frac{\beta_i}{12}\left(\tilde{Y}_{21,i}\tilde{k}_{x,i} + \tilde{Y}_{22,i}\tilde{k}_{\theta,i} + \tilde{Y}_{23,i}\tilde{k}_{x\theta,i}\right) \tag{23}$$
$$\tilde{M}_{x\theta,i} = \frac{\beta_i}{12}\left(\tilde{Y}_{31,i}\tilde{k}_{x,i} + \tilde{Y}_{32,i}\tilde{k}_{\theta,i} + \tilde{Y}_{33,i}\tilde{k}_{x\theta,i}\right)$$

where $\beta_i = h/R_i$ is the thickness ratio of the $i$th cylindrical shell.

The previous equations will be used in the expressions of the boundary conditions of the $i$th cylindrical shell.

### 3.3. Elastic strain energy

The dimensionless elastic strain energy $\tilde{U}_i$ of the $i$th cylindrical shell, which models the single-walled carbon nanotube, under plane stress hypothesis $(\sigma_z = 0)$, can be expressed as follows [37]:

$$\tilde{U}_i = \frac{1}{2\beta_i}\int_0^1\int_0^{2\pi}\int_{-\beta_i/2}^{+\beta_i/2}\left(\tilde{\sigma}_{x,i}\tilde{\varepsilon}_{x,i} + \tilde{\sigma}_{\theta,i}\tilde{\varepsilon}_{\theta,i} + \tilde{\tau}_{x\theta,i}\tilde{\gamma}_{x\theta,i}\right) d\eta d\theta d\zeta \tag{24}$$

By inserting equations (4) and (5) into Eq. (24), the dimensionless elastic strain energy $\tilde{U}_i$ of the $i$th cylindrical shell, in the case of homogeneous anisotropic elastic material, becomes:

$$\tilde{U}_i = \frac{1}{2}\int_0^1\int_0^{2\pi}\left(\tilde{Y}_{11,i}\tilde{\varepsilon}_{x,0,i}^2 + \tilde{Y}_{12,i}\tilde{\varepsilon}_{x,0,i}\tilde{\varepsilon}_{\theta,0,i} + \tilde{Y}_{13,i}\tilde{\varepsilon}_{x,0,i}\tilde{\gamma}_{x\theta,0,i} + \tilde{Y}_{21,i}\tilde{\varepsilon}_{x,0,i}\tilde{\varepsilon}_{\theta,0,i}\right.$$
$$\left.+\tilde{Y}_{22,i}\tilde{\varepsilon}_{\theta,0,i}^2 + \tilde{Y}_{23,i}\tilde{\varepsilon}_{\theta,0,i}\tilde{\gamma}_{x\theta,0,i} + \tilde{Y}_{31,i}\tilde{\varepsilon}_{x,0,i}\tilde{\gamma}_{x\theta,0,i} + \tilde{Y}_{32,i}\tilde{\varepsilon}_{\theta,0,i}\tilde{\gamma}_{x\theta,0,i} + \tilde{Y}_{33,i}\tilde{\gamma}_{x\theta,0,i}^2\right)$$
$$d\eta d\theta + \frac{\beta_i^2}{24}\int_0^1\int_0^{2\pi}\left(\tilde{Y}_{11,i}\tilde{k}_{x,i}^2 + \tilde{Y}_{12,i}\tilde{k}_{x,i}\tilde{k}_{\theta,i} + \tilde{Y}_{13,i}\tilde{k}_{x,i}\tilde{k}_{x\theta,i} + \tilde{Y}_{21,i}\tilde{k}_{x,i}\tilde{k}_{\theta,i}\right.$$
$$\left.+\tilde{Y}_{22,i}\tilde{k}_{\theta,i}^2 + \tilde{Y}_{23,i}\tilde{k}_{\theta,i}\tilde{k}_{x\theta,i} + \tilde{Y}_{31,i}\tilde{k}_{x,i}\tilde{k}_{x\theta,i} + \tilde{Y}_{32,i}\tilde{k}_{\theta,i}\tilde{k}_{x\theta,i} + \tilde{Y}_{33,i}\tilde{k}_{x\theta,i}^2\right) d\eta d\theta \tag{25}$$

In Eq. (25), the first term on the right-hand is associated to the middle surface strains of the shell and represents the stretching energy, while the second one is associated to the middle surface changes in curvature and torsion of the shell and represents the bending energy [42].

The dimensionless elastic strain energy of a DWCNT, given by two concentric SWCNTs, is written in the form [37]:

$$\tilde{U} = \sum_{i=1}^{2}\delta_i\tilde{U}_i \tag{26}$$

where $\delta_i = R_i/R_1$ and $R_1$ is the radius of the inner SWCNT.

### 3.4. Kinetic energy

The dimensional time variable $t$ is made dimensionless by adopting a reference frequency $\omega_0$, which is the lowest extensional circular

frequency of an anisotropic ring under plane strain hypothesis:

$$\omega_0 = \sqrt{\frac{Y}{\rho h R_1^2}} \tag{27}$$

where:

$$Y = \frac{2K_\rho}{3\sqrt{3}} \tag{28}$$

is a reference dimensional surface elastic constant, $\rho$ and $h$ are mass density and thickness of the two layers of the DWCNT, respectively, and $\tau = \omega_0 t$ is the dimensionless time variable.

The dimensionless velocity field of the $i$th cylindrical shell $(\tilde{u}_i', \tilde{v}_i', \tilde{w}_i')$ is written as [37]:

$$\tilde{u}_i' = \frac{d\tilde{u}_i}{d\tau} = \frac{\dot{u}_i}{R_i\omega_0} \qquad \tilde{v}_i' = \frac{d\tilde{v}_i}{d\tau} = \frac{\dot{v}_i}{R_i\omega_0} \qquad \tilde{w}_i' = \frac{d\tilde{w}_i}{d\tau} = \frac{\dot{w}_i}{R_i\omega_0} \quad i = 1,2 \tag{29}$$

where $(\dot{u}_i, \dot{v}_i, \dot{w}_i)$ is the corresponding dimensional velocity field.

The dimensionless kinetic energy of the $i$th cylindrical shell, which models the single-walled carbon nanotube, by neglecting the rotary inertia effect, is given by [37]:

$$\tilde{T}_i = \frac{1}{2}\delta_i^2 \int_0^1 \int_0^{2\pi} (\tilde{u}_i'^2 + \tilde{v}_i'^2 + \tilde{w}_i'^2) d\eta d\theta \quad i = 1,2 \tag{30}$$

The dimensionless kinetic energy of a DWCNT, given by two concentric SWCNTs, is written in the form [37]:

$$\tilde{T} = \sum_{i=1}^{2} \delta_i \tilde{T}_i \tag{31}$$

### 3.5. Van der Waals interaction energy

As previously reported, in the present paper, the actual discrete DWCNTs are modelled by means of couples of concentric equivalent continuous cylindrical shells with van der Waals interactions.

The dimensionless pressure exerted on the $i$th shell due to van der Waals interactions between the two concentric layers $(i, j)$ of the DWCNT can be written as a function of the dimensionless radial displacements $(\tilde{w}_i, \tilde{w}_j)$ of the two layers as follows [29]:

$$\tilde{p}_i(\eta, \theta) = \tilde{c}_{ij}\left(\delta_i \tilde{w}_i - \delta_j \tilde{w}_j\right) \qquad i, j = 1,2 \quad i \neq j \tag{32}$$

where $\tilde{c}_{ij}$ is the dimensionless van der Waals interaction coefficient between the layers $(i, j)$.

This coefficient can be expressed by adopting He's formulation in the form [29]:

$$\tilde{c}_{ij} = -\left(\frac{1001\pi\tilde{\varepsilon}\tilde{\sigma}^{12}}{3\tilde{a}^4}\tilde{E}_{ij}^{13} - \frac{1120\pi\tilde{\varepsilon}\tilde{\sigma}^{6}}{9\tilde{a}^4}\tilde{E}_{ij}^{7}\right)\delta_j \qquad i, j = 1,2 \quad i \neq j \tag{33}$$

where $\varepsilon$ is the C–C potential depth and $\tilde{\varepsilon} = \varepsilon / Y R_1^2$ is the correlated dimensionless parameter, $\sigma$ is the C–C equilibrium distance and $\tilde{\sigma} = \sigma / R_1$ is the correlated dimensionless parameter, and $\tilde{a} = a / R_1$ is the dimensionless C–C bond length.

The dimensionless elliptical integral $\tilde{E}_{ij}^m$ of the expression (33) is written as [29]:

$$\tilde{E}_{ij}^m = (\delta_j + \delta_i)^{-m} \int_0^{\pi/2} \frac{d\theta}{(1 - \tilde{k}_{ij}\cos 2\theta)^{m/2}} \quad i, j = 1,2 \quad i \neq j \quad m = 7, 13 \tag{34}$$

and the dimensionless geometric coefficient $\tilde{k}_{ij}$ is written as [29]:

$$\tilde{k}_{ij} = \frac{4\delta_j\delta_i}{(\delta_j + \delta_i)^2} \quad i, j = 1,2 \quad i \neq j \tag{35}$$

The dimensionless van der Waals interaction energy of the $i$th cylindrical shell, which models the single-walled carbon nanotube, is expressed as follows [29]:

$$\tilde{V}_i = -\frac{1}{2}\delta_i \int_0^1 \int_0^{2\pi} \tilde{p}_i(\eta, \theta)\tilde{w}_i d\eta d\theta \quad i = 1,2 \tag{36}$$

The dimensionless van der Waals interaction energy of a DWCNT, given by two concentric SWCNTs, is written in the form [29]:

$$\tilde{V} = \sum_{i=1}^{2} \delta_i \tilde{V}_i \tag{37}$$

## 4. Vibration modelling of DWCNTs

A modal vibration, i.e. a synchronous motion, of a DWCNT can be formally written as [29]:

$$\begin{aligned} &\tilde{u}_i(\eta, \theta, \tau) = \tilde{U}_i(\eta, \theta)\tilde{f}_i(\tau) \qquad \tilde{v}_i(\eta, \theta, \tau) = \tilde{V}_i(\eta, \theta)\tilde{f}_i(\tau) \\ &\tilde{w}_i(\eta, \theta, \tau) = \tilde{W}_i(\eta, \theta)\tilde{f}_i(\tau) \end{aligned} \qquad i = 1,2 \tag{38}$$

where $(\tilde{U}_i, \tilde{V}_i, \tilde{W}_i)$ are the three dimensionless components of the modal shape of the $i$th cylindrical shell and $\tilde{f}_i(\tau)$ is the corresponding dimensionless time law, which is supposed to be the same for the three dimensionless displacements $(\tilde{u}_i, \tilde{v}_i, \tilde{w}_i)$.

The modal shape components $(\tilde{U}_i, \tilde{V}_i, \tilde{W}_i)$ are expanded by means of a double mixed series in terms of $m$th degree Chebyshev polynomials $T_m^*(\eta)$ along the longitudinal direction $\eta$ and harmonic functions $(\cos n\theta, \sin n\theta)$ along the circumferential direction $\theta$, in the form [29]:

$$\begin{aligned} \tilde{U}_i(\eta, \theta) &= \sum_{m=0}^{M_u}\sum_{n=0}^{N} \tilde{U}_{i,m,n} T_m^*(\eta)\cos n\theta \\ \tilde{V}_i(\eta, \theta) &= \sum_{m=0}^{M_v}\sum_{n=0}^{N} \tilde{V}_{i,m,n} T_m^*(\eta)\sin n\theta \qquad i = 1,2 \\ \tilde{W}_i(\eta, \theta) &= \sum_{m=0}^{M_w}\sum_{n=0}^{N} \tilde{W}_{i,m,n} T_m^*(\eta)\cos n\theta \end{aligned} \tag{39}$$

where $T_m^* = T_m(2\eta - 1)$, $m$ denotes the number of longitudinal half-waves, $n$ represents the number of circumferential waves and $(\tilde{U}_{i,m,n}, \tilde{V}_{i,m,n}, \tilde{W}_{i,m,n})$ are unknown coefficients, which can be obtained by imposing the boundary conditions.

### 4.1. Boundary conditions

In this paper, simply supported, clamped and free DWCNTs are studied; the boundary conditions are imposed applying constraints to the unknown coefficients $(\tilde{U}_{i,m,n}, \tilde{V}_{i,m,n}, \tilde{W}_{i,m,n})$ of expansions (39).

#### 4.1.1. Simply supported DWCNTs

In case of simply supported DWCNTs, the boundary conditions are expressed in the form [29]:

$$\tilde{v}_i = 0 \qquad \tilde{w}_i = 0 \qquad \tilde{N}_{x,i} = 0 \qquad \tilde{M}_{x,i} = 0 \qquad \eta = 0,1 \qquad i = 1,2 \tag{40}$$

which represent both geometric (i.e. on the displacements $(\tilde{v}_i, \tilde{w}_i)$) and natural (i.e. on the forces $\tilde{N}_{x,i}$ and moments $\tilde{M}_{x,i}$) conditions.

Starting from conditions (40), by taking into account equations (22), (23) for the dimensionless force and moment resultants, and Eqs. (38) for the dimensionless displacements, together with expansions (39) for the corresponding modal shape components, and assuming axisymmetric circular cylindrical shells without geometric imperfections, the following equations are derived:

$$\begin{aligned} &\sum_{m=0}^{M_v} \tilde{V}_{i,m,n} T_m^*(\eta) = 0 \\ &\sum_{m=0}^{M_w} \tilde{W}_{i,m,n} T_m^*(\eta) = 0 \\ &\sum_{m=0}^{M_u} \tilde{U}_{i,m,n} T_{m,\eta}^*(\eta) = 0 \\ &\sum_{m=0}^{M_w} \tilde{W}_{i,m,n} T_{m,\eta\eta}^*(\eta) = 0 \end{aligned} \qquad n \in [0, N] \quad \theta \in [0, 2\pi] \quad \eta = 0,1 \quad i = 1,2 \tag{41}$$

where $(\cdot)_{,\eta} = \partial(\cdot)/\partial\eta$ and $(\cdot)_{,\eta\eta} = \partial^2(\cdot)/\partial\eta^2$.

The linear algebraic system given by Eqs. (41) can be solved analytically in terms of the coefficients $(\tilde{U}_{i,1,n}, \tilde{U}_{i,2,n}, \tilde{V}_{i,0,n}, \tilde{V}_{i,1,n}, \tilde{W}_{i,0,n}, \tilde{W}_{i,1,n}, \tilde{W}_{i,2,n}, \tilde{W}_{i,3,n})$, for $n \in [0, N]$. Therefore, in case of simply supported DWCNTs, eight different coefficients for each SWCNT are obtained.

#### 4.1.2. Clamped–clampedDWCNTs

In case of clamped–clamped DWCNTs, the boundary conditions are expressed in the form [29]:

$$\tilde{u}_i = 0 \qquad \tilde{v}_i = 0 \qquad \tilde{w}_i = 0 \qquad \tilde{w}_{i,\eta} = 0 \qquad \eta = 0, 1 \quad i = 1, 2 \tag{42}$$

which all represent geometric (i.e. on the displacements $(\tilde{u}_i, \tilde{v}_i, \tilde{w}_i)$ and velocities $(\tilde{w}_{i,\eta})$) conditions.

Starting from conditions (42), considering equations (38) for the dimensionless displacements and expansions (39) for the corresponding modal shape components, assuming axisymmetric circular cylindrical shells without geometric imperfections, the following equations are derived:

$$\begin{aligned} &\sum_{m=0}^{M_u} \tilde{U}_{i,m,n} T^*_m(\eta) = 0 \\ &\sum_{m=0}^{M_v} \tilde{V}_{i,m,n} T^*_m(\eta) = 0 \\ &\sum_{m=0}^{M_w} \tilde{W}_{i,m,n} T^*_m(\eta) = 0 \\ &\sum_{m=0}^{M_w} \tilde{W}_{i,m,n} T^*_{m,\eta}(\eta) = 0 \end{aligned} \qquad n \in [0, N] \quad \theta \in [0, 2\pi] \quad \eta = 0, 1 \quad i = 1, 2 \tag{43}$$

The linear algebraic system given by Eqs. (43) can be solved analytically in terms of the coefficients $(\tilde{U}_{i,0,n}, \tilde{U}_{i,1,n}, \tilde{V}_{i,0,n}, \tilde{V}_{i,1,n}, \tilde{W}_{i,0,n}, \tilde{W}_{i,1,n}, \tilde{W}_{i,2,n}, \tilde{W}_{i,3,n})$, for $n \in [0, N]$. Therefore, in case of clamped–clamped DWCNTs, eight different coefficients for each SWCNT are obtained.

#### 4.1.3. Free–freeDWCNTs

In case of free–free DWCNTs, the boundary conditions are expressed in the form [29]:

$$\begin{aligned} &\tilde{N}_{x,i} = 0 \qquad \tilde{N}_{x\theta,i} + \tilde{M}_{x\theta,i} = 0 \qquad \tilde{Q}_{x,i} + \frac{\partial \tilde{M}_{x\theta,i}}{\partial \theta} = 0 \\ &\tilde{M}_{x,i} = 0 \qquad \eta = 0, 1 \qquad i = 1, 2 \end{aligned} \tag{44}$$

It can be noted that the boundary conditions (44), applied at the free edges of DWCNTs, are of "natural type" (forces and moments) and not of "geometric type" (displacements and velocities). Since in Rayleigh–Ritz method, which is used in this paper to solve the equations of motion, only the "geometric type" boundary conditions have to be exactly satisfied, while the "natural type" boundary conditions are satisfied by the total energy minimization of the system, then no boundary conditions are imposed in the present work in case of free–free DWCNTs, see Ref. [28] for more details.

### 4.2. Rayleigh–Ritz method

In the case of DWCNTs, the maximum number of variables needed to describe a general vibration mode with $n$ circumferential waves is given by $N_p = 2 \times (M_u + M_v + M_w + 3 - p)$, where 2 is the number of concentric SWCNTs, $M_u = M_v = M_w$ is the maximum number of longitudinal half-waves considered and $p$ is the number of equations needed to satisfy the boundary conditions; in the case of DWCNTs with simply supported, clamped and free boundary conditions it is imposed $p = (8, 8, 0)$, respectively, see Section 4.1 for the details.

Moreover, since the accuracy of applying Ritz method depends strongly on the choice of the modal shape functions, then a convergence analysis was carried out to determine the correct order of Chebyshev orthogonal polynomials: from this analysis, it was found that $M_u = M_v = M_w = 11$ provides accurate results with a relatively reduced computational effort. Starting from the previous observations, for simply supported, clamped and free DWCNTs it is obtained the maximum number of variables $N_p = (56, 56, 72)$, respectively.

For a multi-mode analysis including different values of circumferential waves $n$, the number of degrees of freedom of the system is computed by the relation $N_{\max} = N_p \times (N+1)$, where $N$ is the maximum number of circumferential waves considered.

Eqs. (38) are inserted in the expressions of elastic strain energy (25), kinetic energy (30) and van der Waals interaction energy (36) in order to calculate the value of Rayleigh quotient $R(\tilde{\mathbf{q}})$, where $\tilde{\mathbf{q}}$ is a vector containing all the unknown coefficients of expansions (39), expressed as [37]:

$$\tilde{\mathbf{q}} = \begin{bmatrix} \vdots \\ \tilde{U}_{i,m,n} \\ \tilde{V}_{i,m,n} \\ \tilde{W}_{i,m,n} \\ \vdots \end{bmatrix} \qquad i = 1, 2 \tag{45}$$

After imposing the stationarity to Rayleigh quotient, the following classic eigenvalue problem in dimensionless form is obtained [37]:

$$\left(-\tilde{\omega}^2 \tilde{\mathbf{M}} + \tilde{\mathbf{K}}\right) \tilde{\mathbf{q}} = 0 \tag{46}$$

which provides approximate dimensionless circular frequencies (eigenvalues $\tilde{\omega}_j$) and modal shapes (eigenvectors $\tilde{\mathbf{q}}_j$), with $j = (1, 2, \ldots, N_{\max})$, where $\tilde{\mathbf{M}}$ and $\tilde{\mathbf{K}}$ are the dimensionless mass and stiffness matrices, respectively.

The approximate modal shape of the $j$th mode of the $i$th shell is provided by the expansions (39), where coefficients $(\tilde{U}_{i,m,n}, \tilde{V}_{i,m,n}, \tilde{W}_{i,m,n})$ are replaced with coefficients $(\tilde{U}^{(j)}_{i,m,n}, \tilde{V}^{(j)}_{i,m,n}, \tilde{W}^{(j)}_{i,m,n})$, which are the components of the $j$th eigenvector $\tilde{\mathbf{q}}$ of Eq. (46), and the vector function [37]:

$$\tilde{\mathbf{W}}^{(j)}(\eta, \theta) = \begin{bmatrix} \tilde{U}^{(j)}_i(\eta, \theta) \\ \tilde{V}^{(j)}_i(\eta, \theta) \\ \tilde{W}^{(j)}_i(\eta, \theta) \end{bmatrix} \qquad i = 1, 2 \tag{47}$$

is the approximation of the $j$th eigenfunction vector of the original problem.

### 4.3. Characteristic equation of simply supported anisotropic thin cylindrical shells

Three different circular frequencies $\omega_{i,m,n}$ are associated with every vibration mode $(m, n)$ of a thin cylindrical shell: the lowest one $\omega_{1,m,n}$ is usually associated with the mode where the transversal (i.e. radial) component dominates, while the other two frequencies $(\omega_{2,m,n}, \omega_{3,m,n})$ are usually higher by one order of magnitude and they are associated with the mode where the tangential (i.e. longitudinal and circumferential) components dominate, see Ref. [39].

In the specific case of a thin cylindrical shell of finite length $L$ with simply supported boundary conditions, it is possible to obtain the exact value of the three circular frequencies associated with the generic vibration mode of the shell by computing the roots of the dimensionless characteristic equation (see Ref. [39] for the details of the procedure to obtain the corresponding dimensional equation):

$$\tilde{\omega}^6 - \left(\tilde{K}_2 + \varphi k \Delta \tilde{K}_2\right) \tilde{\omega}^4 + \left(\tilde{K}_1 + \varphi k \Delta \tilde{K}_1\right) \tilde{\omega}^2 - \left(\tilde{K}_0 + \varphi k \Delta \tilde{K}_0\right) = 0 \tag{48}$$

In Eq. (48), $(\tilde{K}_0, \tilde{K}_1, \tilde{K}_2)$ are dimensionless constant coefficients deriving from Donnell shell theory. By considering the anisotropic elastic shell model previously reported, coefficient $\tilde{K}_2$ is written in the form (the same procedure can be extended to the other two coefficients $\tilde{K}_0$ and $\tilde{K}_1$):

$$\begin{aligned} \tilde{K}_2 = {} & \tilde{Y}_{22} + \left(\tilde{Y}_{11} + \tilde{Y}_{33}\right) \lambda^2 + 2\left(\tilde{Y}_{13} + \tilde{Y}_{23}\right) \lambda n + \left(\tilde{Y}_{22} + \tilde{Y}_{33}\right) n^2 \\ & + k\left(\tilde{Y}_{11} \lambda^4 - 4\tilde{Y}_{13} \lambda^3 n + 2\left(\tilde{Y}_{12} + 2\tilde{Y}_{33}\right) \lambda^2 n^2 - 4\tilde{Y}_{32} \lambda n^3 + \tilde{Y}_{22} n^4\right) \end{aligned} \tag{49}$$

where $\lambda$ is the dimensionless axial wavelength parameter [39]:

$$\lambda = \frac{m\pi R}{L} = m\pi\alpha, \quad m = 1, 2, \ldots \tag{50}$$

and $k$ is the dimensionless thickness parameter (which is small in case of thin shells) [39]:

$$k = \frac{h^2}{12R^2} = \frac{1}{12}\beta^2 \tag{51}$$

Again, in Eq. (48), $(\Delta\tilde{K}_0, \Delta\tilde{K}_1, \Delta\tilde{K}_2)$ are modifying dimensionless constant coefficients coming from another shell theory, in the present work Sanders shell theory. By using the anisotropic elastic shell model previously reported, coefficient $\Delta\tilde{K}_2$ is written in the form (the same procedure can be extended to the other two coefficients $\Delta\tilde{K}_0$ and $\Delta\tilde{K}_1$):

$$\Delta\tilde{K}_2 = \frac{9}{4}\tilde{Y}_{33}\lambda^2 + 3\alpha\tilde{Y}_{23}\lambda n + \left(\frac{1}{4}\tilde{Y}_{33} + \tilde{Y}_{22}\right)n^2 \tag{52}$$

Finally, in Eq. (48), $\tilde{\omega}^2$ is the dimensionless frequency parameter of the shell, as:

$$\tilde{\omega}^2 = \frac{\omega^2}{\omega_0^2} \tag{53}$$

where $\omega^2$ is the dimensional frequency parameter of the shell [39] and $\omega_0$ is the reference frequency adopted in the kinetic energy, see Eq. (27), and $\varphi$ is the previously introduced artificial control parameter for the application of Sanders ($\varphi = 1$) or Donnell ($\varphi = 0$) shell theory in the characteristic Eq. (48).

Therefore, starting from the three dimensionless frequency parameters $\tilde{\omega}^2$ of the characteristic Eq. (48), we can get six different dimensionless circular frequencies $\tilde{\omega}$ (three positive and three negative, with the same modulus), where the lowest positive (i.e. fundamental) circular frequency $\tilde{\omega}_1$ is usually associated with a primarily radial (flexural) motion of the considered simply supported thin cylindrical shell of finite length.

## 5. Numerical results

In the present work, natural frequencies of DWCNTs obtained via Donnell and Sanders shell theories are compared. He's formulation is adopted to simulate van der Waals interaction forces between the two concentric SWCNTs. An anisotropic elastic shell model is used to take into account the chirality effects of CNTs. Simply supported, clamped and free boundary conditions are considered. Vibration modes with different number of waves along longitudinal and circumferential directions are analysed. DWCNTs with different aspect ratios are investigated.

In Table 1, the values of C–C bond parameters $(a, k_\rho, k_\theta)$, C–C distance parameters $(\varepsilon, \sigma)$ and CNT equivalent parameters $(h, \rho)$ retrieved from the pertinent literature are reported. In particular, parameters $k_\rho$ and $k_\theta$, which denote force constants related to the variance of C–C bond length $a$ and angle $\theta$, respectively, are used to compute the anisotropic elastic properties of SWCNTs by means of the molecular mechanics "stick-spiral model", see Ref. [53] for more details. Moreover, in order to study the actual discrete DWCNT as a couple of concentric equivalent continuous cylindrical shells, an equivalent thickness $h$, which is derived from MD simulations of CNT energy, and an equivalent mass density $\rho$, resulting from the surface density of graphite, are considered [54].

### 5.1. Accuracy of isotropic vs. anisotropic elastic shell model for SWCNTs

In order to justify the validity of the previous anisotropic elastic shell model, let us consider also the corresponding isotropic model, in which the SWCNT is assumed to be an isotropic elastic thin shell, with tensile rigidity $C$ (in-plane stiffness), bending rigidity $D$ (flexural stiffness), surface density $\sigma$ (mass density $\rho$ per unit lateral area $h$ of the SWCNT) and Poisson's ratio $\nu$ reported in Table 2.

The first important aspect to be clarified is which of the isotropic or anisotropic elastic shell models is more accurate, and therefore should be adopted in the following comparisons between the natural frequencies of DWCNTs.

**Table 1**
Mechanical parameters adopted in the anisotropic elastic shell model [54].

| | |
|---|---|
| **C-C bond parameters** | |
| C-C bond length $a$(nm) | 0.142 |
| C-C bond elongation $K_\rho$(nN/nm) | 742 |
| C-C bond angle variance $K_\theta$(nN · nm) | 1.42 |
| **C-C distance parameters** | |
| C-C potential depth $\varepsilon(10^{-22}$ J) | 4.755 |
| C-C equilibrium separation distance $\sigma$(nm) | 0.3407 |
| **CNT equivalent parameters** | |
| Thickness $h$(nm) | 0.066 |
| Mass density $\rho$(kg/m$^3$) | 11700 |

**Table 2**
Mechanical parameters adopted in the isotropic elastic shell model [25].

| | |
|---|---|
| Tensile rigidity $C$ (J/m$^2$) | 360 |
| Bending rigidity $D$ (J) | $1.362 \times 10^{-19}$ |
| Surface density $\sigma$ (kg/m$^2$) | $7.718 \times 10^{-7}$ |
| Poisson's ratio $\nu$ | 0.19 |

To this aim, in this Section, the results of the isotropic and anisotropic elastic shell models are compared with experimental data available in the literature from the resonant Raman spectroscopy in terms of natural frequencies of radial breathing modes (RBMs).

RBM is a vibration mode that is used to identify experimentally SWCNTs by resonant Raman spectroscopy. This mode, which corresponds to the wavenumbers ($m = 0, n = 0$) and is referred to as "Rayleigh's inextensional mode", appears only in the case of free–free boundary conditions and is independent from the SWCNT length [8,9].

In order to perform a correct analysis, the same shell theory should be adopted: in this Section, Sanders shell theory is adopted, but the same results would be obtained via Donnell shell theory.

In Table 3, natural frequencies of the RBM for free–free SWCNTs with different diameters $D$ and constant aspect ratio $L/D = 10$ obtained by means of resonant Raman spectroscopy are compared with those obtained considering isotropic and anisotropic elastic models and adopting Sanders shell theory, where experimental data are considered as the reference (they are actual results). From Table 3, it is noted that the anisotropic elastic shell model is more accurate than the isotropic one, as it gives natural frequencies closer to the ones of the resonant Raman spectroscopy; therefore, in the following, the anisotropic elastic shell model will be adopted to obtain natural frequencies of CNTs.

This result is due to the fact that, actually, CNTs are discrete systems, i.e., they are intrinsically non-isotropic, and therefore an anisotropic model, which is able to take into account chirality effects, should be adopted to properly study their vibration characteristics, see Ref. [52] for more details.

### 5.2. Accuracy of Sanders vs. Donnell shell theory for SWCNTs

The second fundamental aspect to be clarified is which of Sanders or Donnell shell theories is more accurate, and therefore should be assumed as the reference in the following comparisons between the natural frequencies of DWCNTs.

To this aim, in this Section, the results of Sanders and Donnell shell theories are compared with numerical data available in the literature from molecular dynamics simulations (MDS) in terms of natural frequencies of beam-like modes (BLMs).

BLM is a specific vibration mode that cannot be experimentally identified via resonant Raman spectroscopy, but it can only be determined computationally by means of finite element (FE) analyses or MDS. In particular, this mode corresponds to only one circumferential

**Table 3**
Natural frequencies of the radial breathing mode ($m = 0, n = 0$). Free–free SWCNTs with different diameters $D$ and constant aspect ratio $L/D = 10$. Comparisons between resonant Raman spectroscopy (reference data), isotropic elastic shell model (see Table 2) and anisotropic elastic shell model (see Table 1) considering Sanders shell theory.

| Natural frequency (THz) | | Difference (%) | |
|---|---|---|---|
| Diameter $D$ (nm) | Resonant Raman spectroscopy [10] | Isotropic elastic model (Sanders shell theory) | Anisotropic elastic model (Sanders shell theory) |
| 1.01796 | 7.165 | 3.63 | 1.09 |
| 1.03587 | 7.105 | 4.50 | 1.13 |
| 1.05348 | 6.865 | 2.85 | 1.00 |
| 1.13743 | 6.295 | 1.87 | 0.56 |
| 1.40948 | 5.276 | 4.76 | 1.19 |
| 1.41599 | 5.216 | 4.83 | 1.69 |
| 1.43534 | 5.066 | 3.37 | 1.01 |
| 1.46703 | 4.947 | 3.21 | 0.80 |
| 1.49190 | 4.917 | 4.19 | 1.47 |
| 1.52844 | 4.797 | 4.23 | 1.23 |
| 1.54043 | 4.737 | 3.76 | 0.94 |
| 1.56413 | 4.677 | 3.91 | 1.37 |
| 1.59902 | 4.617 | 4.85 | 1.45 |
| 1.62752 | 4.527 | 4.62 | 1.15 |
| 1.64439 | 4.437 | 3.74 | 1.31 |
| 1.69398 | 4.317 | 4.04 | 1.21 |

wave ($n = 1$) and is related to bending vibrations of beams, plates and shells in the presence of simply supported, clamped or free boundary conditions [40].

MDS allow the free vibrations of SWCNTs with different geometries and boundary conditions to be studied by taking into account atomic structure and potential energy of the carbon atoms. The interaction between the carbon atoms is specified by adopting energy potentials associated with bond stretching, changes in the angle between adjacent bonds, bond torsion and inversion, van der Waals interactions, coupling among stretching, bending and torsional deformations [11,12].

In order to perform a correct analysis, for both the shell theories considered, in this Section the anisotropic elastic shell model is used, since it was proven to be more accurate than the isotropic one for the vibration modelling of CNTs.

In Table 4, natural frequencies of BLMs in case of clamped–clamped SWCNTs with constant diameter $D = 0.658$ nm and different aspect ratios $L/R$ obtained via MDS are compared with those obtained by adopting Donnell and Sanders shell theories and considering the anisotropic elastic shell model, where MDS data are considered as the reference (they are obtained by considering CNTs as discrete anisotropic structures and therefore they are very close to actual results).

From Table 4, it is noted that Sanders shell theory is more accurate than Donnell shell theory, as it gives, for different vibration modes and geometries, natural frequencies closer to the ones of the molecular dynamics simulations; therefore, in the following, Sanders shell theory will be considered as the reference in the vibration modelling of DWCNTs.

Moreover, from Table 4, it is noted that, for the first four beam-like modes, as the length of SWCNT increases, the percentage difference between Sanders shell theory and MDS decreases, while the percentage difference between Donnell shell theory and MDS increases; therefore, it is found that the accuracy of Sanders shell theory increases while the accuracy of Donnell shell theory decreases with increasing SWCNT length.

### 5.3. Applicability and limitations of Donnell shell theory for DWCNTs

In the present Section, starting from the previously reported results, natural frequencies of DWCNTs obtained via Donnell and Sanders shell theories are compared. He's formulation is applied to simulate van der Waals interaction forces between the two concentric SWCNTs. An anisotropic elastic shell model is adopted to take into account CNT chirality effects. Simply supported boundary conditions are applied. Vibration modes with different number of waves along longitudinal and circumferential directions are analysed. DWCNTs with different aspect ratios are investigated.

The aim is to study applicability and limitations of Donnell shell theory, compared to the more accurate Sanders shell theory, which is adopted as reference, for vibration modelling of DWCNTs.

Let us consider a DWCNT composed by two concentric SWCNTs with radius $R_1 = 5.00$ nm (inner SWCNT), which corresponds to chirality indices $(r_1, s_1) = (74, 74)$, and $R_2 = 5.34$ nm (outer SWCNT), which corresponds to chirality indices $(r_2, s_2) = (79, 79)$, i.e., an armchair DWCNT: by using the value of CNT equivalent thickness $h = 0.066$ nm reported in Table 1, it is derived that the value of thickness-to-radius ratio of both the concentric SWCNTs, i.e. $h/R_1 = 0.0132$ for the inner one and $h/R_2 = 0.0124$ for the outer one, is comprised in the validity range $0.002 \leq h/R \leq 0.05$ of "Love's first approximation" assumptions [39]. Therefore, the two concentric SWCNTs can be modelled as thin cylindrical shells, and Donnell and Sanders shell theories can be applied to obtain the natural frequencies of the considered DWCNT, whose mechanical parameters are listed in Table 5, where $\rho$ is the mass density of CNTs and $Y$ is a reference elastic constant, see Eq. (28).

Starting from the mechanical parameters reported in Table 5 and considering Eq. (6), the anisotropic surface elastic constants $Y_{jk,i}$, which take into account the chirality effects of CNTs and are inserted into the anisotropic elastic constitutive equations (5), are obtained in the present case of armchair DWCNT, see Table 6.

From Table 6, the most relevant features of the anisotropic surface elastic constant matrix $\boldsymbol{Y}$ of a SWCNT can be observed, where the first is that the surface elastic constant along the longitudinal direction is identical to the one along the circumferential direction, i.e., $Y_{11,i} = Y_{22,i}$, and the second is that the matrix $\boldsymbol{Y}$ is symmetric, i.e., $Y_{12,i} = Y_{21,i}$, $Y_{13,i} = Y_{31,i}$, $Y_{23,i} = Y_{32,i}$, see Ref. [54].

Moreover, since an armchair DWCNT is considered in the present paper, then it is obtained that $Y_{13,i} = Y_{31,i} = Y_{23,i} = Y_{32,i} = 0$, see Ref. [54].

The previous relations between surface elastic constants are identical to those in an isotropic material, and the graphene sheet is indeed isotropic. However, CNTs are actually anisotropic due to the curvature effect. This can be verified by the fact that the surface elastic constant $Y_{33,i}$, which is the shear modulus of the $i$-th SWCNT, cannot be related to the other elastic constants of the same SWCNT as in isotropic elasticity.

Furthermore, from Table 6, according to Ref. [58], it is obtained that, for sufficiently large diameters, as in the present case, the two SWCNTs have the same values of the corresponding surface elastic constants. These values for CNTs tend asymptotically to the corresponding

**Table 4**
Natural frequencies of beam-like modes ($n = 1$). Clamped–clamped SWCNTs with constant diameter $D = 0.678$ nm and different aspect ratios $L/R$. Comparisons between molecular dynamics simulations (reference data), Sanders shell theory and Donnell shell theory considering the anisotropic elastic shell model (see Table 1).

| Natural frequency (THz) | | Difference (%) | |
|---|---|---|---|
| $L/R = 10.52$ | | | |
| Vibration mode $(m, n)$ | Molecular dynamics simulations [13] | Sanders shell theory (anisotropic model) | Donnell shell theory (anisotropic model) |
| (1, 1) | 0.975 | 3.09 | 9.73 |
| (2, 1) | 2.105 | 2.89 | 5.02 |
| (3, 1) | 3.404 | 2.57 | 3.84 |
| (4, 1) | 4.724 | 1.99 | 3.00 |
| $L/R = 15.60$ | | | |
| Vibration mode $(m, n)$ | Molecular dynamics simulations [13] | Sanders shell theory (anisotropic model) | Donnell shell theory (anisotropic model) |
| (1, 1) | 0.538 | 1.04 | 20.2 |
| (2, 1) | 1.246 | 1.30 | 6.01 |
| (3, 1) | 2.090 | 1.51 | 3.68 |
| (4, 1) | 2.993 | 1.31 | 2.76 |
| $L/R = 20.68$ | | | |
| Vibration mode $(m, n)$ | Molecular dynamics simulations [13] | Sanders shell theory (anisotropic model) | Donnell shell theory (anisotropic model) |
| (1, 1) | 0.336 | 0.21 | 42.1 |
| (2, 1) | 0.818 | 0.17 | 9.73 |
| (3, 1) | 1.417 | 0.60 | 4.49 |
| (4, 1) | 2.079 | 0.61 | 2.86 |

**Table 5**
Constant mechanical parameters of the considered simply supported armchair DWCNT.

| | |
|---|---|
| Inner radius $R_1$(nm) | 5.00 |
| Outer radius $R_2$(nm) | 5.34 |
| Thickness $h$(nm) | 0.066 |
| Mass density $\rho$(kg/m$^3$) | 11700 |
| Surface elastic constant $Y$(nN/nm) | 285.60 |

**Table 6**
Anisotropic surface elastic constants of the considered simply supported armchair DWCNT.

| Anisotropic surface elastic constant $Y_{jk,i}$ | Numerical value (nN/nm) |
|---|---|
| Inner SWCNT | |
| $Y_{11,1} = Y_{22,1}$ | 369.61 |
| $Y_{12,1} = Y_{21,1}$ | 58.780 |
| $Y_{13,1} = Y_{31,1}$ | 0 |
| $Y_{23,1} = Y_{32,1}$ | 0 |
| $Y_{33,1}$ | 155.38 |
| Outer SWCNT | |
| $Y_{11,2} = Y_{22,2}$ | 369.62 |
| $Y_{12,2} = Y_{21,2}$ | 58.778 |
| $Y_{13,2} = Y_{31,2}$ | 0 |
| $Y_{23,2} = Y_{32,2}$ | 0 |
| $Y_{33,2}$ | 155.39 |

values of graphite, i.e., $Y_{11} = Y_{22} = 369.46$ nN/nm and $Y_{12} = Y_{21} = 59.113$ nN/nm.

In Tables 7–9, natural frequencies of the simply supported DWCNT of Table 5 with constant aspect ratio $L/R_2 = 10$ obtained by means of Donnell and Sanders shell theories and considering the anisotropic elastic model are listed. Axisymmetric ($n = 0$), beam-like ($n = 1$) and circumferential flexural ($n = 2$) vibration modes are studied. The number of longitudinal half-waves $1 \leq m \leq 5$ is analysed. Vibration modes with prevalent longitudinal $u$, circumferential $v$ or radial $w$ displacement component, which corresponds to a primarily axial (i.e., tensile or compression), torsional or flexural vibration, respectively, are investigated.

From these comparisons, it is noted that almost all percentage differences are equal to zero. The only relevant exceptions to the previous observation are given by the lowest natural frequencies corresponding to the modal shape with prevalent radial $w$ displacement of the circumferential flexural modes ($n = 2$), which present a relatively high percentage difference ($\approx 8\%$). This value decreases with increasing the number of longitudinal half-waves until $m = 5$, which has a negligible percentage difference ($= 0.05\%$). Therefore, it is obtained that the difference in the results due to the different shell theory (Sanders vs. Donnell) considered to model the vibration characteristics of DWCNTs is concentrated in the lowest radial natural frequencies of circumferential flexural modes with relatively low number of longitudinal half-waves.

By preserving the number of longitudinal half-waves $1 \leq m \leq 5$, let us extend the previous analyses by considering the number of circumferential waves $0 \leq n \leq 8$ and the value of aspect ratio $10 \leq L/R_2 \leq 50$. In addition, on the basis of the previously obtained results, let us focus our attention on the lowest radial natural frequencies.

In Figs. 3–7, the curves of the percentage differences between the natural frequencies of the simply supported DWCNT of Table 5 obtained by considering Donnell and Sanders shell theories are shown, where the more accurate Sanders shell theory is assumed as reference. The anisotropic elastic shell model is adopted. Different wavenumbers and aspect ratios are considered.

From Fig. 3, the following observations for the aspect ratio $L/R_2 = 10$ can be made:

- for $n = (0, 1)$ the percentage difference is equal to zero for every value of $m$ and an excellent agreement between Donnell and Sanders shell theories is present;
- for $2 \leq n \leq 6$ the percentage difference is different for every value of $m$ and a disagreement between Donnell and Sanders shell theories is clearly seen. In particular, for every value of $n$, the highest percentage difference is present for $m = 1$, then it decreases with increasing $m$. At the same time, with increasing the value of $m$, the peak of the percentage difference curve moves towards increasing values of $n$ and reduces its value. Therefore it is derived that, in the range $2 \leq n \leq 6$, the disagreement between the two shell theories increases with decreasing the values of $m$ and $n$;
- for $n = (7, 8)$ the percentage difference is negligible ($\leq 2\%$) and almost equal for every value of $m$, this difference reduces

**Table 7**
Natural frequencies (THz) of the simply supported DWCNT of Table 5. Aspect ratio $L/R_2 = 10$.
Anisotropic model. Comparisons between Donnell and Sanders shell theories. Axisymmetric modes ($n = 0$).

| Natural frequency (THz) | | | | Difference (%) |
|---|---|---|---|---|
| Vibration mode $(m, n)$ | Prevalent displacement | Donnell shell theory (anisotropic model) | Sanders shell theory (anisotropic model) | |
| (1,0) | $v$ | 0.1119 | 0.1119 | 0.00 |
| | $v$ | 0.1119 | 0.1119 | 0.00 |
| | $u$ | 0.1722 | 0.1722 | 0.00 |
| | $u$ | 0.1755 | 0.1755 | 0.00 |
| | $w$ | 0.5791 | 0.5791 | 0.00 |
| | $w$ | 2.3428 | 2.3428 | 0.00 |
| (2,0) | $v$ | 0.2237 | 0.2237 | 0.00 |
| | $v$ | 0.2237 | 0.2237 | 0.00 |
| | $u$ | 0.3416 | 0.3416 | 0.00 |
| | $u$ | 0.3511 | 0.3511 | 0.00 |
| | $w$ | 0.5840 | 0.5840 | 0.00 |
| | $w$ | 2.3428 | 2.3428 | 0.00 |
| (3,0) | $v$ | 0.3356 | 0.3356 | 0.00 |
| | $v$ | 0.3356 | 0.3356 | 0.00 |
| | $u$ | 0.4916 | 0.4916 | 0.00 |
| | $u$ | 0.5267 | 0.5267 | 0.00 |
| | $w$ | 0.6087 | 0.6087 | 0.00 |
| | $w$ | 2.3429 | 2.3429 | 0.00 |
| (4,0) | $v$ | 0.4474 | 0.4474 | 0.00 |
| | $v$ | 0.4474 | 0.4474 | 0.00 |
| | $w$ | 0.5505 | 0.5505 | 0.00 |
| | $u$ | 0.7022 | 0.7022 | 0.00 |
| | $u$ | 0.7249 | 0.7249 | 0.00 |
| | $w$ | 2.3430 | 2.3430 | 0.00 |
| (5,0) | $v$ | 0.5596 | 0.5596 | 0.00 |
| | $v$ | 0.5596 | 0.5596 | 0.00 |
| | $w$ | 0.5602 | 0.5602 | 0.00 |
| | $u$ | 0.8778 | 0.8778 | 0.00 |
| | $u$ | 0.8904 | 0.8904 | 0.00 |
| | $w$ | 2.3432 | 2.3432 | 0.00 |

**Table 8**
Natural frequencies (THz) of the simply supported DWCNT of Table 5. Aspect ratio $L/R_2 = 10$.
Anisotropic model. Comparisons between Donnell and Sanders shell theories. Beam-like modes ($n = 1$).

| Natural frequency (THz) | | | | Difference (%) |
|---|---|---|---|---|
| Vibration mode $(m, n)$ | Prevalent displacement | Donnell shell theory (anisotropic model) | Sanders shell theory (anisotropic model) | |
| (1,1) | $w$ | 0.0333 | 0.0333 | 0.00 |
| | $u$ | 0.3790 | 0.3790 | 0.00 |
| | $u$ | 0.4106 | 0.4106 | 0.00 |
| | $v$ | 0.5862 | 0.5862 | 0.00 |
| | $v$ | 0.8266 | 0.8266 | 0.00 |
| | $w$ | 2.3474 | 2.3474 | 0.00 |
| (2,1) | $w$ | 0.1065 | 0.1065 | 0.00 |
| | $u$ | 0.4250 | 0.4250 | 0.00 |
| | $u$ | 0.4942 | 0.4942 | 0.00 |
| | $v$ | 0.6620 | 0.6620 | 0.00 |
| | $v$ | 0.8520 | 0.8520 | 0.00 |
| | $w$ | 2.3475 | 2.3475 | 0.00 |
| (3,1) | $w$ | 0.1888 | 0.1888 | 0.00 |
| | $u$ | 0.4908 | 0.4908 | 0.00 |
| | $u$ | 0.5921 | 0.5921 | 0.00 |
| | $v$ | 0.7706 | 0.7706 | 0.00 |
| | $v$ | 0.9014 | 0.9014 | 0.00 |
| | $w$ | 2.3477 | 2.3477 | 0.00 |
| (4,1) | $w$ | 0.2667 | 0.2667 | 0.00 |
| | $u$ | 0.5713 | 0.5713 | 0.00 |
| | $u$ | 0.6832 | 0.6832 | 0.00 |
| | $v$ | 0.9000 | 0.9000 | 0.00 |
| | $v$ | 0.9827 | 0.9827 | 0.00 |
| | $w$ | 2.3480 | 2.3480 | 0.00 |
| (5,1) | $w$ | 0.3346 | 0.3346 | 0.00 |
| | $u$ | 0.6615 | 0.6615 | 0.00 |
| | $u$ | 0.7639 | 0.7639 | 0.00 |
| | $v$ | 1.0425 | 1.0425 | 0.00 |
| | $v$ | 1.0957 | 1.0957 | 0.00 |
| | $w$ | 2.3484 | 2.3484 | 0.00 |

**Table 9**
Natural frequencies (THz) of the simply supported DWCNT of Table 5. Aspect ratio $L/R_2 = 10$.
Anisotropic model. Comparisons between Donnell and Sanders shell theories. Beam-like modes ($n = 1$).

| Natural frequency (THz) | | | | Difference (%) |
|---|---|---|---|---|
| Vibration mode $(m, n)$ | Prevalent displacement | Donnell shell theory (anisotropic model) | Sanders shell theory (anisotropic model) | |
| (1,2) | ***w*** | **0.0139** | **0.0128** | **8.59** |
| | $u$ | 0.7232 | 0.7232 | 0.00 |
| | $u$ | 0.7710 | 0.7710 | 0.00 |
| | $v$ | 1.1183 | 1.1183 | 0.00 |
| | $v$ | 1.3079 | 1.3079 | 0.00 |
| | $w$ | 2.3656 | 2.3656 | 0.00 |
| (2,2) | ***w*** | **0.0434** | **0.0431** | **0.70** |
| | $u$ | 0.7524 | 0.7524 | 0.00 |
| | $u$ | 0.8030 | 0.8030 | 0.00 |
| | $v$ | 1.1596 | 1.1596 | 0.00 |
| | $v$ | 1.3342 | 1.3342 | 0.00 |
| | $w$ | 2.3660 | 2.3660 | 0.00 |
| (3,2) | ***w*** | **0.0871** | **0.0870** | **0.11** |
| | $u$ | 0.7938 | 0.7938 | 0.00 |
| | $u$ | 0.8544 | 0.8544 | 0.00 |
| | $v$ | 1.2248 | 1.2248 | 0.00 |
| | $v$ | 1.3785 | 1.3785 | 0.00 |
| | $w$ | 2.3667 | 2.3667 | 0.00 |
| (4,2) | ***w*** | **0.1369** | **0.1368** | **0.07** |
| | $u$ | 0.8456 | 0.8456 | 0.00 |
| | $u$ | 0.9183 | 0.9183 | 0.00 |
| | $v$ | 1.3100 | 1.3100 | 0.00 |
| | $v$ | 1.4415 | 1.4415 | 0.00 |
| | $w$ | 2.3678 | 2.3678 | 0.00 |
| (5,2) | ***w*** | **0.1878** | **0.1877** | **0.05** |
| | $u$ | 0.9072 | 0.9072 | 0.00 |
| | $u$ | 0.9888 | 0.9888 | 0.00 |
| | $v$ | 1.4113 | 1.4113 | 0.00 |
| | $v$ | 1.5226 | 1.5226 | 0.00 |
| | $w$ | 2.3693 | 2.3693 | 0.00 |

with increasing the value of $n$, and therefore a close agreement between Donnell and Sanders shell theories is present.

In Figs. 4–6, the value of aspect ratio $L/R_2$ of the simply supported DWCNT of Table 5 is increased from $L/R_2 = 20$ to $L/R_2 = 30$ and to $L/R_2 = 40$, respectively.

From Fig. 7, the following comments for the aspect ratio $L/R_2 = 50$ can be made:

- for $n = 0$ the percentage difference is equal to zero for every value of $m$ and therefore an excellent agreement between Donnell and Sanders shell theories is present;
- for $1 \leq n \leq 3$ the percentage difference is different for every value of $m$ and a corresponding strong disagreement between Donnell and Sanders shell theories is clearly seen. In particular, for every value of $n$, the highest percentage difference is present for $m = 1$, then it decreases with increasing $m$. At the same time, with increasing the value of $m$, the peak of the curve of percentage difference moves towards increasing values of $n$ and reduces its value. Therefore it is obtained that within the range $1 \leq n \leq 3$ the disagreement between the two shell theories increases with decreasing the values of $m$ and $n$;
- for $4 \leq n \leq 6$ the percentage difference is not negligible (as it is comprised between 6% and 8%) and almost equal for every value of $m$, where this difference reduces with increasing the value of $n$, and a sensible disagreement between Donnell and Sanders shell theories is present;
- for $n = (7, 8)$ the percentage difference is negligible ($\leq$ 2%) and almost equal for every value of $m$, this difference reduces with increasing the value of $n$, and therefore a close agreement between Donnell and Sanders shell theories is present.

In order to compare the previous results, in Fig. 8 the curves of the percentage differences of Fig. 3 (aspect ratio $L/R_2 = 10$) and Fig. 7 (aspect ratio $L/R_2 = 50$) are plotted together.

From Fig. 8, the following observations for increasing aspect ratios $L/R_2$ can be made:

- the number of circumferential waves $n$ with zero percentage difference for every number of longitudinal half-waves $m$ reduces its range from $n = (0, 1)$ to $n = 0$;
- the number of circumferential waves $n$ with different percentage difference for every number of longitudinal half-waves $m$ reduces its range from $2 \leq n \leq 6$ to $1 \leq n \leq 3$;
- within the range of $n$ with different percentage difference for every value of $m$, the value of every $m$th percentage difference curve increases;
- within the range of $n$ with different percentage difference for every value of $m$, the peak of every $m$th percentage difference curve moves towards decreasing values of $n$ and increases its value;
- the number of circumferential waves $n$ presenting very close percentage difference for every number of longitudinal half-waves $m$ enlarges its range from $n = (7, 8)$ to $4 \leq n \leq 8$;
- within the range $n = (7, 8)$ the percentage difference curves are almost coincident.

Therefore, assuming the more accurate Sanders shell theory as the reference, and considering the anisotropic elastic shell model, from Figs. 3–8, with respect to the number of circumferential waves $n$, as a function of the value of aspect ratio $L/R_2$ and of the number of longitudinal half-waves $m$, the following ranges of applicability of Donnell shell theory for vibration modelling of DWCNTs are identified:

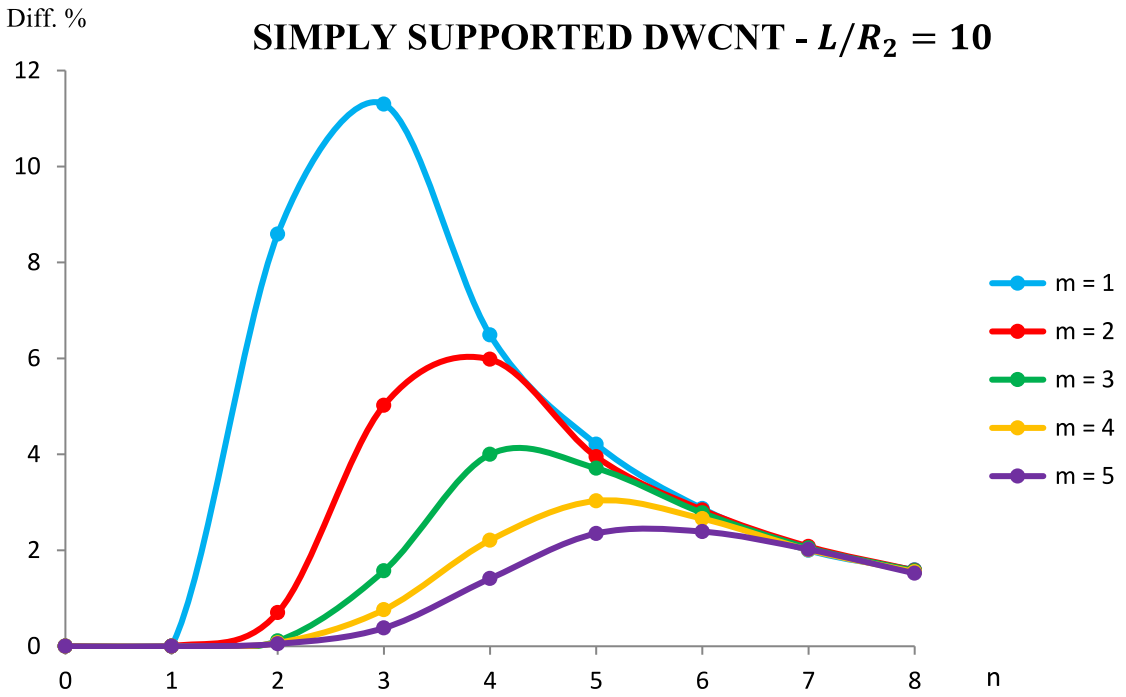


**Fig. 3.** Percentage differences between the natural frequencies obtained by applying Donnell and Sanders shell theories (Sanders as reference). Anisotropic elastic shell model. Simply supported DWCNT of Table 5 with aspect ratio $L/R_2 = 10$. Number of longitudinal half-waves $m$. Number of circumferential waves $n$.

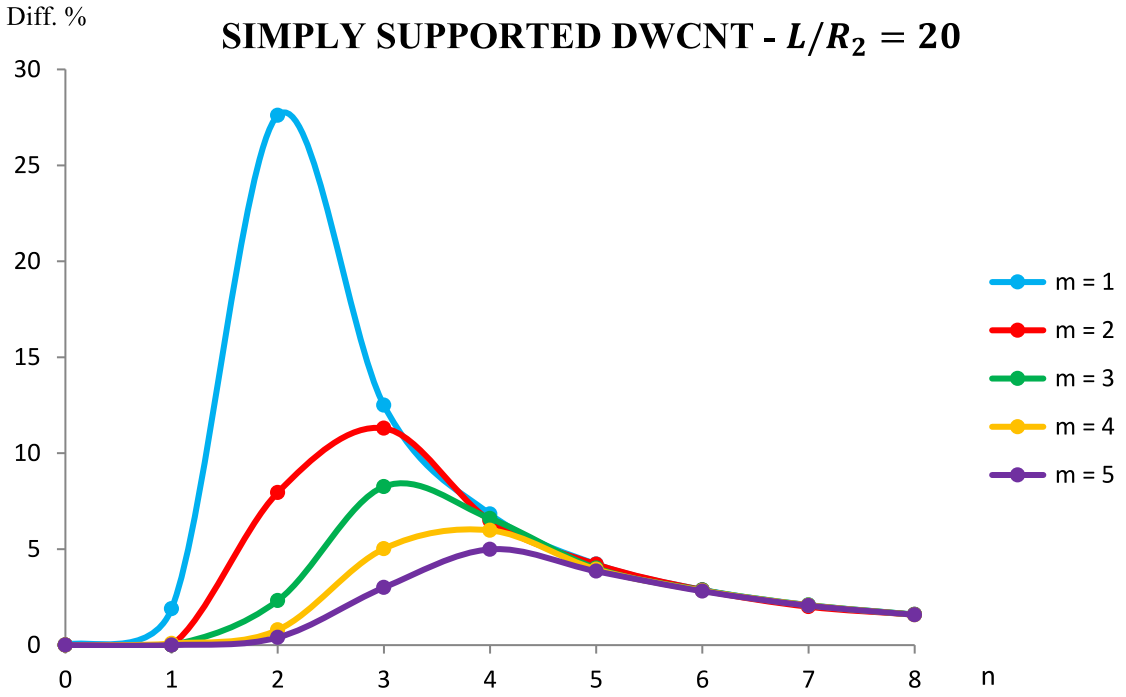


**Fig. 4.** Percentage differences between the natural frequencies obtained by applying Donnell and Sanders shell theories (Sanders as reference). Anisotropic elastic shell model. Simply supported DWCNT of Table 5 with aspect ratio $L/R_2 = 20$. Number of longitudinal half-waves $m$. Number of circumferential waves $n$.

- $n = 0$ (axisymmetric modes), for every value of $L/R_2$ and $m$;
- $n = 1$ (beam-like modes), for relatively low values of $L/R_2$ and relatively high values of $m$;
- $n = (7, 8)$ (shell-like modes with relatively high values of $n$), for every value of $L/R_2$ and $m$

while the corresponding limitations of Donnell shell theory for vibration modelling of DWCNTs are:

- $n = 1$ (beam-like modes), for relatively high values of $L/R_2$ and relatively low values of $m$;
- $2 \leq n \leq 6$ (shell-like modes with relatively low values of $n$), for every value of $L/R_2$ and $m$

where the percentage differences between the natural frequencies increase with increasing the value of aspect ratio $L/R_2$ and with decreasing the number of longitudinal half-waves $m$ and circumferential

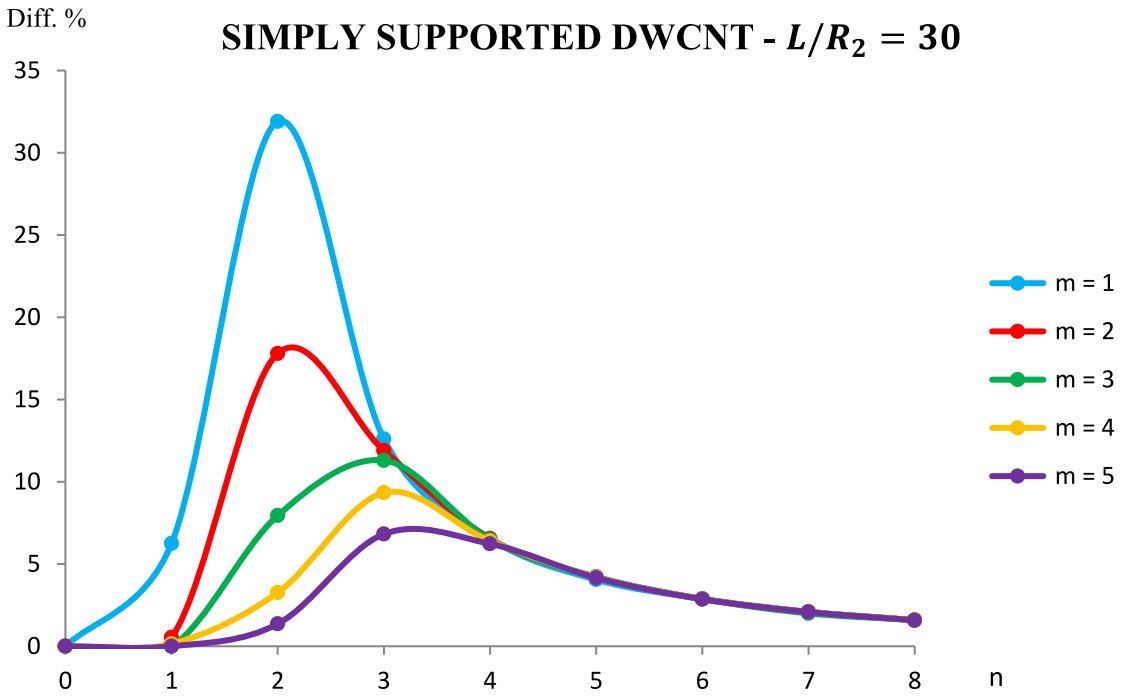


**Fig. 5.** Percentage differences between the natural frequencies obtained by applying Donnell and Sanders shell theories (Sanders as reference). Anisotropic elastic shell model. Simply supported DWCNT of Table 5 with aspect ratio $L/R_2 = 30$. Number of longitudinal half-waves $m$. Number of circumferential waves $n$.

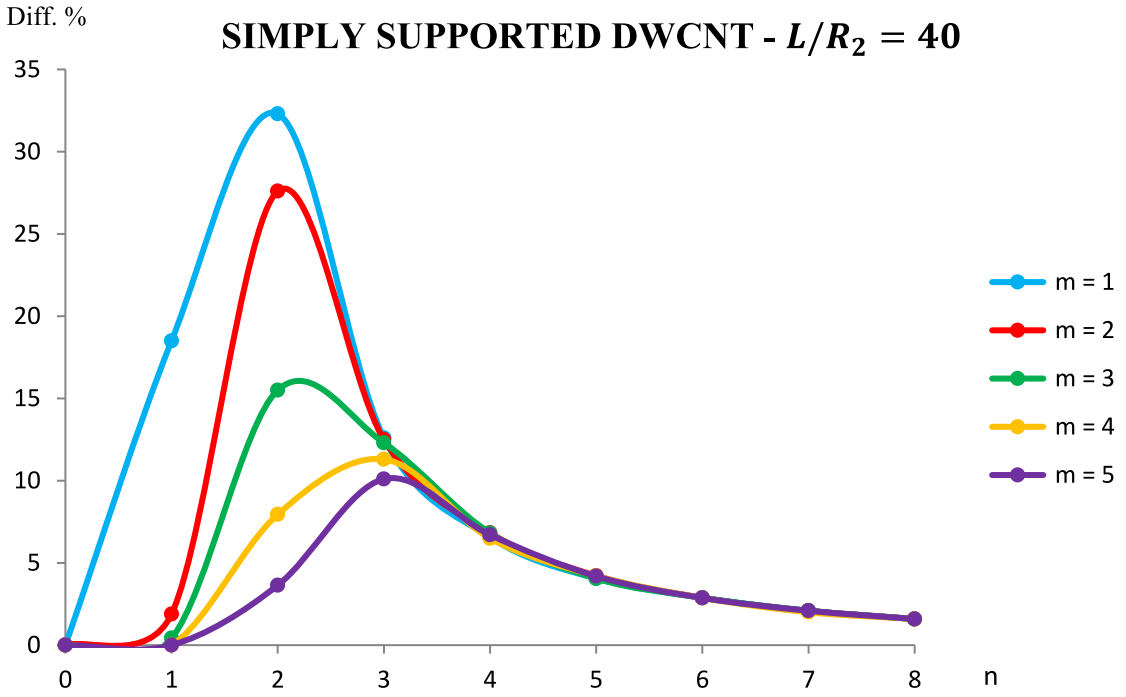


**Fig. 6.** Percentage differences between the natural frequencies obtained by applying Donnell and Sanders shell theories (Sanders as reference). Anisotropic elastic shell model. Simply supported DWCNT of Table 5 with aspect ratio $L/R_2 = 40$. Number of longitudinal half-waves $m$. Number of circumferential waves $n$.

waves $n$ (in these cases the accuracy of Donnell shell theory reduces).

### *5.4. Limitations of Donnell shell theory in vibration modelling of thin cylindrical shells*

In this Section, we want to justify analytically the numerical results obtained in Section 5.3 for simply supported DWCNTs on the basis of Eq. (48)–(53) defined for simply supported anisotropic thin cylindrical shells of finite length.

Let us consider the dimensionless constant coefficient $\tilde{K}_2$ (49) from Donnell shell theory and the modifying dimensionless constant coefficient $\Delta\tilde{K}_2$ (52) from Sanders shell theory that are written by considering the previously reported anisotropic elastic shell model, and focus our attention on their ratio $\Delta\tilde{K}_2/\tilde{K}_2$, which denotes the difference between Sanders and Donnell shell theories [39] (it must be stressed

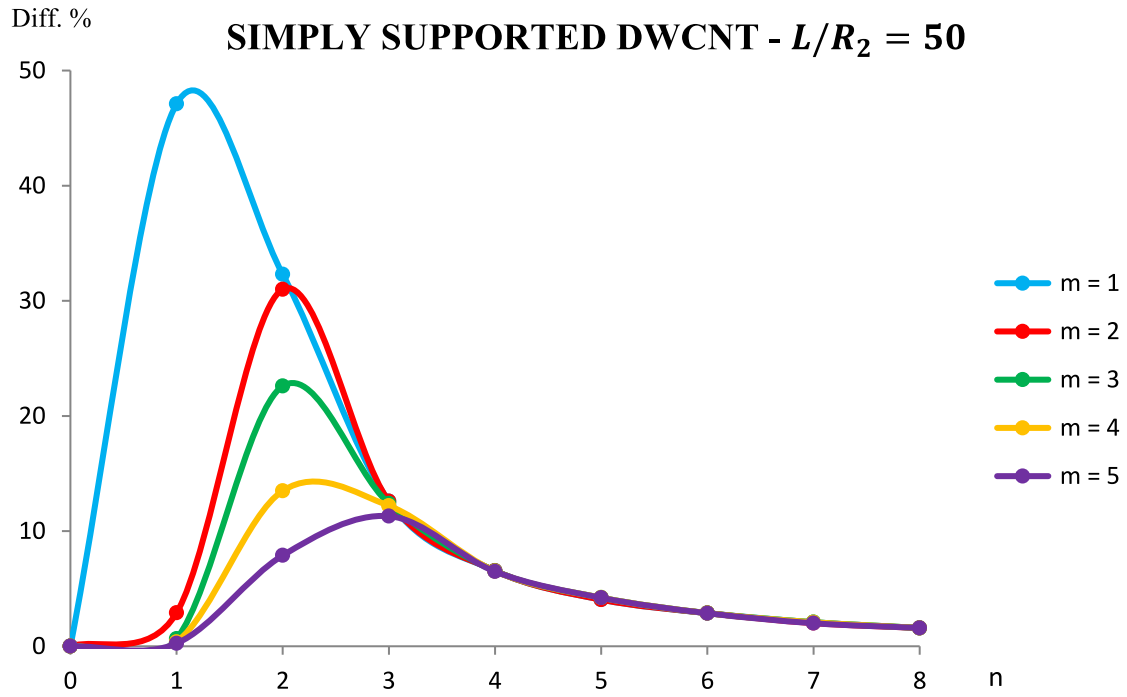


**Fig. 7.** Percentage differences between the natural frequencies obtained by applying Donnell and Sanders shell theories (Sanders as reference). Anisotropic elastic shell model. Simply supported DWCNT of Table 5 with aspect ratio $L/R_2 = 50$. Number of longitudinal half-waves $m$. Number of circumferential waves $n$.

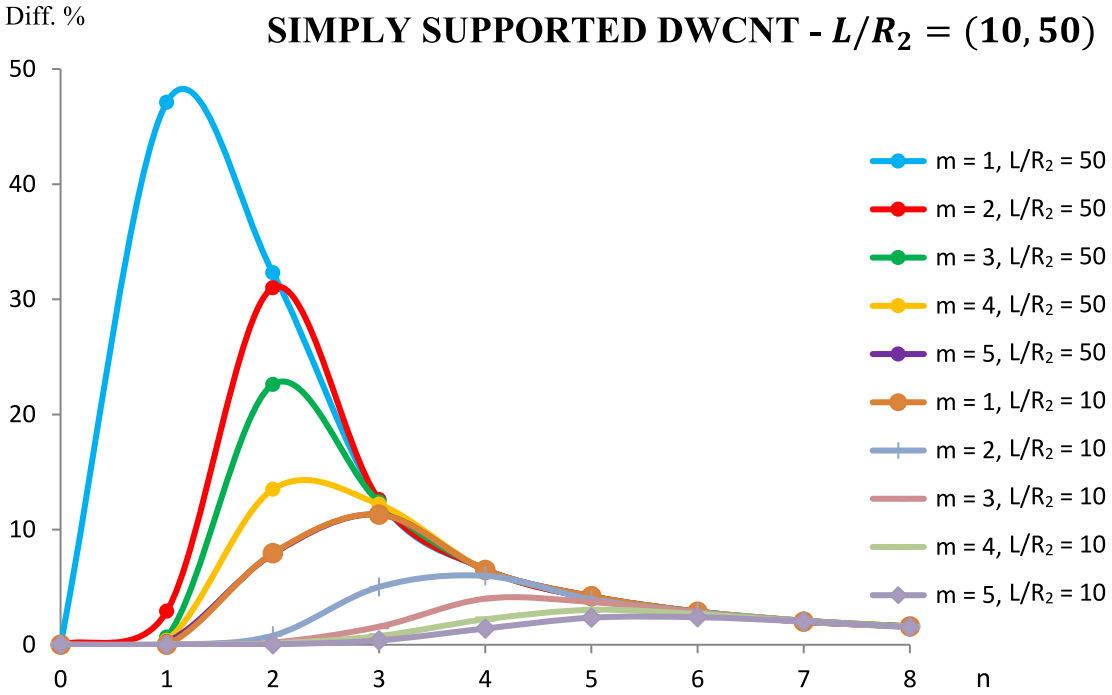


**Fig. 8.** Percentage differences between the natural frequencies obtained by applying Donnell and Sanders shell theories (Sanders as reference). Anisotropic elastic shell model. Simply supported DWCNT of Table 5 with aspect ratios $L/R_2 = (10, 50)$. Number of longitudinal half-waves $m$. Number of circumferential waves $n$.

that the same procedure can be extended to the other two pairs of coefficients).

With respect to the number of circumferential waves $n$, from Eq. (49) it can be observed that the constant coefficient $\tilde{K}_2$ is of the same order of $k \times n^4$, where $k$ is the dimensionless thickness parameter (51), while from Eq. (52) it can be observed that the modifying constant coefficient $\Delta\tilde{K}_2$ is of the same order of $n^2$. Therefore, the ratio $\Delta\tilde{K}_2/\tilde{K}_2$ results of the same order of $1/(k \times n^2)$. Considering $n = 1$ (beam-like modes), the ratio $\Delta\tilde{K}_2/\tilde{K}_2$ is equal to $1/k$ and a substantial difference between Sanders and Donnell shell theories is present; by increasing the value of $n$, with $n > 1$ (shell-like modes), the ratio $\Delta\tilde{K}_2/\tilde{K}_2$ decreases, and it becomes negligible for relatively high values of $n$. This analytical consideration for thin cylindrical shells confirms the numerical results obtained in Section 5.3 for DWCNTs, i.e., the differences between the

natural frequencies computed by applying Donnell and Sanders shell theories reduce with increasing the number of circumferential waves $n$.

Concerning with the number of longitudinal half-waves $m$, from Eq. (50) it can be seen that, for a constant value of radius-to-length ratio $R/L$, $m$ is directly proportional to the dimensionless axial wavelength parameter $\lambda$; moreover, since from Eq. (49) it can be noted that the constant coefficient $\tilde{K}_2$ is of the same order of $k \times \lambda^4$, and from Eq. (52) it is observed that the modifying constant coefficient $\Delta\tilde{K}_2$ is of the same order of $\lambda^2$, then the ratio $\Delta\tilde{K}_2/\tilde{K}_2$ results of the same order of $1/(k \times \lambda^2)$. Therefore, for relatively low values of $m$ (or $\lambda$), the ratio $\Delta\tilde{K}_2/\tilde{K}_2$ is not negligible and a significant difference between Sanders and Donnell shell theories is present; on the other hand, by increasing the value of $m$, the ratio $\Delta\tilde{K}_2/\tilde{K}_2$ decreases, and it becomes negligible for relatively high values of $m$. Also this last analytical consideration for thin cylindrical shells confirms the numerical results obtained in Section 5.3 for DWCNTs, i.e., the differences between the natural frequencies computed by applying Donnell and Sanders shell theories reduce with increasing the number of longitudinal half-waves $m$.

As for the aspect ratio $L/R$, from Eq. (50) it can be derived that, for a constant number of longitudinal half-waves $m$, $L/R$ is inversely proportional to the dimensionless axial wavelength parameter $\lambda$; moreover, as previously observed also for $m$, the ratio $\Delta\tilde{K}_2/\tilde{K}_2$ results of the same order of $1/(k \times \lambda^2)$. Therefore, for relatively low values of $L/R$, the ratio $\Delta\tilde{K}_2/\tilde{K}_2$ is almost negligible; by increasing the value of $L/R$, the ratio $\Delta\tilde{K}_2/\tilde{K}_2$ increases, and it becomes non negligible for relatively high values of $L/R$, with a substantial difference between Sanders and Donnell shell theories. This last analytical consideration for thin cylindrical shells confirms again the numerical results obtained in Section 5.3 for DWCNTs, i.e., the differences between the natural frequencies computed by using Donnell and Sanders shell theories increase with increasing the value of aspect ratio $L/R$.

As, for $n = 0$ (axisymmetric modes), the modifying constant coefficient $\Delta\tilde{K}_2$ (52) of Sanders shell theory depends only on $\lambda^2$, then for relatively high values of aspect ratio $L/R$ this coefficient can be neglected, and the two shell theories in case of axisymmetric modes are in perfect agreement for every value of $m$.

The last two results, the one on aspect ratio $L/R$ and the other on axisymmetric modes $n = 0$, are both due to the fact that the difference between the two shell theories is concentrated in only two deformation terms, i.e., the dimensionless middle surface change in curvature $\tilde{k}_{\theta,i}$ and torsion $\tilde{k}_{x\theta,i}$ of the $i$th shell, which are both present in the bending energy, while there is no difference between the two shell theories in terms of dimensionless middle surface strains, which are all contained in the membrane energy, see equations (2,3,25).

Since in the axisymmetric modes ($n = 0$) the contribution of the bending energy is zero (the elastic strain energy of the DWCNT coincides with the membrane energy), then the two shell theories overlap, and their percentage difference is equal to zero for every number of longitudinal half-waves $m$ and for every value of aspect ratio $L/R_2$.

On the contrary, as in the asymmetric modes ($n \geq 1$) the contribution of the bending energy is much greater than the contribution of the membrane energy, and the bending energy contribution increases as the length $L$ of the DWCNT increases, then the two shell theories do not coincide, and their percentage difference increases as the value of the aspect ratio $L/R_2$ increases.

Therefore, the previous analytical considerations developed for thin cylindrical shells confirm and justify the numerical results obtained in Section 5.3 on applicability and limitations of Donnell shell theory for vibration modelling of DWCNTs.

## 6. Conclusions

In this paper, natural frequencies of simply supported, clamped and free DWCNTs obtained by using Donnell and Sanders shell theories are compared. The discrete DWCNTs are modelled by means of couples of concentric continuous thin cylindrical shells, where van der Waals interactions between layers are simulated via He's formulation. Rayleigh–Ritz method is considered to obtain approximate natural frequencies and modal shapes. Different values of aspect ratio $L/R_2$ are investigated. Different numbers of longitudinal half-waves $m$ and circumferential waves $n$ are analysed. The more accurate Sanders shell theory is assumed as reference. The more accurate and also realistic anisotropic elastic shell model is adopted within the constitutive equations. The main findings are reported below:

- the difference in the results due to the different shell theory (Donnell vs. Sanders) considered to model the discrete DWCNT as a couple of concentric continuous thin cylindrical shells is localized in the lowest radial natural frequencies;
- for $n = 0$ (axisymmetric modes) the two shell theories are in perfect agreement for every value of aspect ratio ($10 \leq L/R_2 \leq 50$) and every number of longitudinal half-waves ($1 \leq m \leq 5$);
- for $n = 1$ (beam-like modes) the two shell theories are in close agreement for relatively low values of aspect ratio ($10 \leq L/R_2 \leq 20$) and for numbers of longitudinal half-waves $2 \leq m \leq 5$;
- for $n = 1$ (beam-like modes) Donnell shell theory is in substantial error for relatively high values of aspect ratio ($30 \leq L/R_2 \leq 50$) and for the number of longitudinal half-waves $m = 1$;
- for $2 \leq n \leq 6$ (shell-like modes with relatively low number of circumferential waves) Donnell shell theory is in substantial error for every value of aspect ratio ($10 \leq L/R_2 \leq 50$) and for every number of longitudinal half-waves ($1 \leq m \leq 5$);
- for $n = (7,8)$ (shell-like modes with relatively high number of circumferential waves) the two shell theories are in close agreement for every value of aspect ratio ($10 \leq L/R_2 \leq 50$) and for every number of longitudinal half-waves ($1 \leq m \leq 5$).

Therefore, Donnell shell theory cannot be used in vibration modelling of DWCNTs for:

- $n = 1$ in case of relatively long shells ($30 \leq L/R_2 \leq 50$) and for $m = 1$;
- $2 \leq n \leq 6$ over the entire considered range of aspect ratios ($10 \leq L/R_2 \leq 50$) and of numbers of longitudinal half-waves ($1 \leq m \leq 5$).

Conversely, Donnell shell theory can be used in vibration modelling of DWCNTs for:

- $n = 0$ over the entire considered range of aspect ratios ($10 \leq L/R_2 \leq 50$) and of numbers of longitudinal half-waves ($1 \leq m \leq 5$);
- $n = 1$ for relatively short shells ($10 \leq L/R_2 \leq 20$) and for $2 \leq m \leq 5$;
- $n = (7,8)$ over the entire considered range of aspect ratios ($10 \leq L/R_2 \leq 50$) and of numbers of longitudinal half-waves ($1 \leq m \leq 5$).

Moreover, the differences between the natural frequencies of DWCNTs obtained by applying Donnell and Sanders shell theories increase with increasing the aspect ratio $L/R_2$ and with decreasing the number of longitudinal half-waves $m$ and the number of circumferential waves $n$. In these cases, since Donnell shell theory results less accurate, one has to use Sanders shell theory.

The previous results obtained for DWCNTs confirm the limitations of Donnell shell theory in vibration modelling of thin cylindrical shells with respect to Sanders shell theory.

### CRediT authorship contribution statement

**Matteo Strozzi:** Writing – review & editing, Writing – original draft, Visualization, Validation, Software, Resources, Methodology, Investigation, Data curation, Conceptualization. **Isaac E. Elishakoff:** Writing –

review & editing, Writing – original draft, Visualization, Validation, Project administration, Methodology, Investigation, Formal analysis, Conceptualization. **Leonid I. Manevitch:** Supervision, Methodology, Investigation, Conceptualization. **Oleg V. Gendelman:** Supervision, Conceptualization.

## Declaration of Competing Interest

The authors declare that they have no known competing financial interests or personal relationships that could have appeared to influence the work reported in this paper.

## Acknowledgements

The Authors would like to express sincere gratitude to Professor Marco Amabili (McGill University, Canada) for the valuable suggestions and references on applicability and limitations of Donnell shell theory in vibration modelling of thin cylindrical shells.

The Authors are grateful to Israel Science Foundation (Grant n. 1696/17) for the financial support of the present work.

This research was initiated when the co-Author Isaac E. Elishakoff served as Visiting Distinguished Professor at the Faculty of Civil and Environmental Engineering at the Technion – Israel Institute of Technology (Haifa), under sponsorship by the Edmond J. Safra Foundation, in Summer 2018.

In the same period, co-Authors Leonid I. Manevitch and Matteo Strozzi served as Visiting Professor and Visiting Post-Doctoral Fellow, respectively, at the Faculty of Mechanical Engineering at the Technion – Israel Institute of Technology (Haifa), under invitation and supervision of the co-Author Oleg V. Gendelman.

With very much sadness of the other co-Authors, after severe illness, Professor Leonid I. Manevitch died on August 20, 2020, at the age of 82. Professor Manevitch followed the research presented in this paper with great attention to the end, dispensing useful suggestions on mathematical modelling and pointing out very interesting comparative works in literature. The co-Authors therefore want to dedicate this work to the blessed memory of Professor Leonid I. Manevitch, outstanding educator, respected teacher, admired scholar.

## References

[1] I. Elishakoff, D. Pentaras, K. Dujat, C. Versaci, G. Muscolino, J. Storch, S. Bucas, N. Challamel, T. Natsuki, Y.Y. Zhang, C.M. Wang, G. Ghyselinck, Carbon Nanotubes and Nano Sensors: Vibrations, Buckling, and Ballistic Impact, ISTE-Wiley, London, 2012.

[2] S. Chakraverty, L. Behera, Static and Dynamic Problems of Nanobeams and Nanoplates, World Scientific, Singapore, 2017.

[3] K.M. Liew, Y. Jianwei, L. Zhang, Mechanical Behaviors of Carbon Nanotubes: Theoretical and Numerical Approaches, Elsevier, Amsterdam, 2017.

[4] K.I. Tserpes, N. Silvestre, Modeling of Carbon Nanotubes, Graphene and their Composites, Springer International Publishing, Switzerland, 2014.

[5] V. Harik, Trends in Nanoscale Mechanics: Mechanics of Carbon Nanotubes, Graphene, Nanocomposites and Molecular Dynamics, Springer, Dordrecht, 2014.

[6] A. Rahman, I. Ali, S.M. Al Zahrani, R. Eleithy, A review of the applications of nanocarbon polymer composites, NANO Brief Report Review, 6, 2011, pp. 185–203.

[7] E.T. Thostenson, Z. Ren, T.W. Chou, Advances in the science and technology of carbon nanotubes and their composites: A review, Compos. Sci. Technol. 61 (2001) 1899–1912.

[8] A.M. Rao, E. Richter, S. Bandow, B. Chase, P. Eklund, K. Williams, S. Fang, K. Subbaswamy, M. Menon, A. Thess, R. Smalley, G. Dresselhaus, M.S. Dresselhaus, Diameter-selective Raman scattering from vibrational modes in carbon nanotubes, Science 275 (1997) 187–191.

[9] S. Bandow, S. Asaka, Y. Saito, A.M. Rao, L. Grigorian, E. Richter, P.C. Eklund, Effect of the growth temperature on the diameter distribution and chirality of single-wall carbon nanotubes, Phys. Rev. Lett. 80 (1998) 3779–3782.

[10] A. Jorio, R. Saito, J.H. Hafner, C.M. Lieber, M. Hunter, T. McClure, G. Dresselhaus, M.S. Dresselhaus, Structural (n, m) determination of isolated single-wall carbon nanotubes by resonant Raman scattering, Phys. Rev. Lett. 86 (2001) 1118–1121.

[11] S. Gupta, F.G. Bosco, R.C. Batra, Breakdown of structural models for vibrations of single-wall zigzag carbon nanotubes, J. Appl. Phys. 106 (2009) 063527.

[12] H.C. Cheng, Y.L. Liu, C. Wu, W.H. Chen, On radial breathing vibration of carbon nanotubes, Comput. Methods Appl. Mech. Eng. 199 (2010) 2820–2827.

[13] W.H. Duan, C.M. Wang, Y.Y. Zhang, Calibration of nonlocal scaling effect parameter for free vibration of carbon nanotubes by molecular dynamics, J. Appl. Phys. 101 (2007) 024305.

[14] I. Elishakoff, D. Pentaras, Fundamental natural frequencies of double-walled carbon nanotubes, J. Sound Vib. 322 (2009) 652–664.

[15] D. Pentaras, I. Elishakoff, Free vibration of triple-walled carbon nanotubes, Acta Mech. 221 (2011) 239–249.

[16] K.Y. Xu, X.N. Guo, C.Q. Ru, Vibration of a double-walled carbon nanotube aroused by nonlinear intertube van der Waals forces, J. Appl. Phys. 99 (2006) 064303(7).

[17] T. Natsuki, Q.Q. Ni, M. Endo, Analysis of the vibration characteristics of double-walled carbon nanotubes, Carbon 46 (2008) 1570–1573.

[18] B. Ravi Kumar, Investigation on mechanical vibration of double-walled carbon nanotubes with inter-tube van der Waals forces, Adv. Nano Res. 6 (2018) 135–145.

[19] C.Q. Ru, Column buckling of multi-walled carbon nanotubes with interlayer radial displacements, Phys. Rev. B 62 (2000) 16962–16967.

[20] J. Yoon, C.Q. Ru, A. Mioduchowski, Terahertz vibration of short carbon nanotubes modeled as Timoshenko beams, J. Appl. Mech. 72 (2005) 10–17.

[21] C.M. Wang, V.B.C. Tan, Y.Y. Zhang, Timoshenko beam model for vibration analysis of multi-walled carbon nanotubes, J. Sound Vib. 294 (2006) 1060–1072.

[22] L.L. Ke, Y. Xiang, J. Yang, S. Kitipornchai, Nonlinear free vibration of embedded double-walled carbon nanotubes based on nonlocal Timoshenko beam theory, Comput. Mater. Sci. 47 (2009) 409–417.

[23] Y.G. Hu, K.M. Liew, Q. Wang, Nonlocal elastic beam models for flexural wave propagation in double-walled carbon nanotubes, J. Appl. Phys. 106 (2009) 044301(6).

[24] D. Pentaras, I. Elishakoff, Effective Approximations for natural frequencies of double-walled carbon nanotubes based on Donnell shell theory, J. Nanotechnol. Eng. Med. 2 (2011) 021013(4).

[25] M. Strozzi, L.I. Manevitch, F. Pellicano, V.V. Smirnov, D.S. Shepelev, Low-frequency linear vibrations of single-walled carbon nanotubes: Analytical and numerical models, J. Sound Vib. 333 (2014) 2936–2957.

[26] M. Amabili, Nonlinear Vibrations of Circular Cylindrical Shells with Different Boundary Conditions, Am. Inst. Aeronaut. Astronaut. J. 41 (2003) 1119–1130.

[27] M. Strozzi, V.V. Smirnov, L.I. Manevitch, F. Pellicano, Nonlinear vibrations and energy exchange of single-walled carbon nanotubes, Radial breathing modes, Compos. Struct. 184 (2018) 613–632.

[28] F. Pellicano, Vibrations of circular cylindrical shells: Theory and experiments, J. Sound Vib. 303 (2007) 154–170.

[29] M. Strozzi, F. Pellicano, Linear vibrations of triple-walled carbon nanotubes, Math. Mech. Solids 23 (2018) 1456–1481.

[30] M. Strozzi, F. Pellicano, Nonlinear Resonance Interaction between Conjugate Circumferential Flexural Modes in Single-Walled Carbon Nanotubes, Shock Vib. (2019) ID 3241698, 33.

[31] C.Y. Wang, L.C. Zhang, An elastic shell model for characterizing single-walled carbon nanotubes, Nanotechnology 19 (2008) 195704(6).

[32] M. Strozzi, V.V. Smirnov, L.I. Manevitch, F. Pellicano, Nonlinear normal modes, resonances and energy exchange in single-walled carbon nanotubes, Int. J. Non-Linear Mech. 120 (2020) 103398(19).

[33] J. Kaplunov, L.I. Manevitch, V.V. Smirnov, Vibrations of an elastic cylindrical shell near the lowest cut-off frequency, Proc. R. Soc. Lond. Ser. A Math. Phys. Eng. Sci. 472 (2018) 20150753.

[34] F. Rizzetto, E. Jansen, M. Strozzi, F. Pellicano, Nonlinear dynamic stability of cylindrical shells under pulsating axial loading via Finite Element analysis using numerical time integration, Thin-Walled Struct. 143 (2019) 106213(16).

[35] X.Q. He, S. Kitipornchai, K.M. Liew, Buckling analysis of multi-walled carbon nanotubes: a continuum model accounting for van der Waals interaction, J. Mech. Phys. Solids 53 (2005) 303–326.

[36] X.Q. He, M. Eisenberger, K.M. Liew, The effect of van der Waals interaction modeling on the vibration characteristics of multiwalled carbon nanotubes, J. Appl. Phys. 100 (2006) 124317(12).

[37] M. Strozzi, O.V. Gendelman, I.E. Elishakoff, F. Pellicano, Applicability and Limitations of Simplified Elastic Shell Theories for Vibration Modelling of Double-Walled Carbon Nanotubes, C - J. Carbon Res. 7 (3) (2021) 1–34, 61.

[38] F. Pellicano, Dynamic instability of a cylindrical shell carrying top mass under base excitation: Experiments and theory, Int. J. Solids Struct. 48 (2011) 408–427.

[39] A.W. Leissa, Vibration of Shells, Acoustical Society of America, Columbus, Ohio, 1993.

[40] W. Soedel, Vibrations of Shells and Plates, Marcel Dekker, Inc., New York, 2004.

[41] E. Ventsel, Thin Plates and Shells. Theory, Analysis, and Applications, Marcel Dekker, Inc., New York, 2001.

[42] M. Amabili, Nonlinear Vibrations and Stability of Shells and Plates, Cambridge University Press, New York, 2008.

[43] M. Amabili, Comparison of shell theories for large-amplitude vibrations of circular cylindrical shells: Lagrangian approach, J. Sound Vib. 264 (2003) 1091–1125.

[44] H.W. Lee, M.K. Kwak, Free vibration analysis of circular cylindrical shell using Rayleigh–Ritz method and comparison of shell theories, J. Sound Vib. 353 (2015) 344–377.
[45] A. Farshidian, P. Oliazad, Free vibration analysis of circular cylindrical shells: comparison of different shell theories, Int. J. Mech. Appl. 2 (2012) 74–80.
[46] N.J. Hoff, Accuracy of Donnell's Equations, J. Appl. Mech. 22 (1955) 329–334.
[47] S.H. Hashemi, M.R. Ilkhani, M. Fadaee, Identification of the validity range of Donnell and Sanders shell theories using an exact vibration analysis of functionally graded thick cylindrical shell panel, Acta Mech. 223 (2012) 1101–1118.
[48] C.Y. Wang, C.Q. Ru, A. Mioduchowski, Applicability and Limitations of Simplified Elastic Shell Equations for Carbon Nanotubes, J. Appl. Mech. 71 (2004) 622–631.
[49] N. Silvestre, C.M. Wang, Y. Zhang, Y. Xiang, Sanders shell model for buckling of single-walled carbon nanotubes with small aspect ratio, Compos. Struct. 93 (2011) 1683–1691.
[50] N. Silvestre, On the accuracy of shell models for torsional buckling of carbon nanotubes, Eur. J. Mech. A Solids 32 (2012) 103–108.
[51] J.G. Teng, T. Hong, Nonlinear thin shell theories for numerical buckling predictions, Thin-Walled Struct. 31 (1998) 89–115.
[52] C.Q. Ru, Chirality-dependent mechanical behaviour of carbon nanotubes based on an anisotropic elastic shell model, Math. Mech. Solids 14 (2009) 88–101.
[53] T. Chang, J. Geng, X. Guo, Prediction of chirality and size-dependent elastic properties of single-walled carbon nanotubes via a molecular mechanics model, Proc. R. Soc. Lond. Ser. A Math. Phys. Eng. Sci. 462 (2006) 2523–2540.
[54] T. Chang, A molecular based anisotropic shell model for single-walled carbon nanotubes, J. Mech. Phys. Solids 58 (2010) 1422–1433.
[55] E. Ghavanloo, S.A. Fazelzadeh, Vibration characteristics of single-walled carbon nanotubes based on an anisotropic elastic shell model, Appl. Math. Model. 36 (2012) 4988–5000.
[56] S.A. Fazelzadeh, E. Ghavanloo, Nonlocal anisotropic elastic shell model for vibrations of single-walled carbon nanotubes with arbitrary chirality, Compos. Struct. 94 (2012) 1016–1022.
[57] C.L. Zhang, H.S. Shen, Temperature-dependent elastic properties of single-walled carbon nanotubes: Prediction from molecular dynamics simulation, Appl. Phys. Lett. 89 (2006) 081904.
[58] C.L. Zhang, H.S. Shen, Predicting the elastic properties of double-walled carbon nanotubes by molecular dynamics simulation, J. Phys. D: Appl. Phys. 41 (2008) 055404.